The Reaction Kinetics of Dimethyl Ether. II: Low Temperature Oxidation in Flow Reactors

H. J. Curran
Chemistry and Materials Science Directorate,
Lawrence Livermore National Laboratory,
Livermore, CA 94551

S. L. Fischer and F. L. Dryer
Department of Mechanical and Aerospace Engineering,
Princeton University,
Princeton, NJ 08544

Accepted to the International Journal of Chemical Kinetics

First submitted on September 3rd 1999,
in final form June 16th 2000.

The Reaction Kinetics of Dimethyl Ether. II: Low Temperature Oxidation in Flow Reactors

H. J. Curran
Chemistry and Materials Science Directorate,
Lawrence Livermore National Laboratory,
Livermore, CA 94551

S. L. Fischer and F. L. Dryer
Department of Mechanical and Aerospace Engineering,
Princeton University,
Princeton, NJ 08544

Abstract

Dimethyl ether oxidation has been studied in a variable-pressure flow reactor over an initial reactor temperature range of 550–850 K, in the pressure range 12–18 atm, at equivalence ratios of $0.7 \leq \phi \leq 4.2$ with nitrogen diluent of approximately 98.5%. On-line extraction sampling in conjunction with FTIR, NDIR (for CO and CO_2), and electrochemical (for O_2) analyses were performed to quantify species at specific locations along the axis of the turbulent flow reactor. Product species concentrations were correlated against residence time (at constant inlet temperature) and against temperature (at fixed mean residence time) in the reactor. Formic acid was observed as a major intermediate of dimethyl ether oxidation at low temperatures. The experimental species evolution profiles were compared to the predictions of a previously published detailed kinetic mechanism [1]. This mechanism did not predict the formation of formic acid. In the current study we have included chemistry leading to formic acid formation (and oxidation). This new chemistry is discussed and is able to reproduce the experimental observations with good accuracy. In addition, this model is able to reproduce low temperature kinetic data obtained in a jet-stirred reactor [2] and the shock tube results of Pfahl et al. [3].

Introduction

In a companion paper [4], we discuss the background as to why dimethyl ether (DME) has been featured in the combustion literature as an alternative for or additive to diesel fuel. In that paper, we considered only the high temperature kinetics, presenting new flow reactor data on the pyrolysis and oxidation of DME at temperatures above 1000 K. We also compared calculated results based upon a new detailed kinetic model with the flow reactor data, and with previously published high temperature oxidation data from a different flow reactor, stirred reactors, and shock tubes.

One of the important attributes of DME as a diesel fuel is its high cetane rating [5]. An understanding of the low and intermediate temperature oxidative behavior is therefore of practical interest. In this paper, we report the new data obtained at low and intermediate temperatures using a variable-pressure flow reactor (VPFR) [6]. These data are then considered along with other low and intermediate temperature kinetic data to further develop

and validate a detailed kinetic model for DME oxidation. A number of prior experimental and modeling works on low and intermediate DME oxidation have appeared previously, and these works are briefly summarized below.

Atmospheric DME oxidation studies [7]–[9] have focused on the reaction of the methoxymethyl-peroxy radical with hydroperoxy radicals [7], the self-reaction of methoxymethyl-peroxy radicals [8], and the reaction of methoxymethyl-peroxy radicals with NO and NO_2 [9]. Sehested et al. [10] studied the self reaction and thermal decomposition of the methoxymethyl radical, in addition to its reaction with molecular oxygen. Masaki et al. [11] and Sehested et al. [12] also studied the rate of methoxymethyl addition to molecular oxygen and measured consistent rate constant expressions. All of these earlier studies were performed at approximately 296 K, a temperature which is much lower than those experienced in operating diesel engines or in diesel engine fuels systems.

More recently, Hoyermann and Nacke [13] studied some elementary reactions of the ethoxymethyl radical in the gas phase, most notably its reactions with molecular and atomic oxygen. These experiments were performed in the temperature range 300–700 K and at pressures of 1–5 mbar. The low pressures of this work leave some doubt as to whether or not the measured rate expression would be valid at high pressures. Finally, Maricq et al. [14] studied the oxidation of DME in the temperature range 230–350 K. They concluded that the reaction between methoxymethyl radical and molecular oxygen proceeds along two distinct pathways. At pressures above about 100 Torr the peroxy radical is predominantly formed. However, as the pressure is reduced, a channel leading to the formation of hydroxyl radical and two formaldehyde molecules becomes progressively more important.

More general mechanistic studies of DME oxidation have also appeared. In 1996, Dagaut et al. [15] reported the first experimental results on the oxidation of DME at high temperatures, including species distribution information as a function of overall residence time. Results were obtained in a jet-stirred reactor (JSR) at 1 and 10 atm, $0.2 \leq \phi \leq 2.5$, and $800 \leq \mathrm{T} \leq 1300$ K. Pfahl and coworkers [3] also measured DME ignition delay times behind reflected shock waves at 13 and 40 bar, $\phi = 1.0$ and $650 \leq \mathrm{T} \leq 1300$ K. Although no species distributions were reported in this work, the results clearly demonstrated that DME exhibits typical "two-stage" ignition characteristics common to many hydrocarbons, that is low temperature, negative temperature coefficient, and hot ignition phenomena. Curran et al. [1] used the combination of the Dagaut et al. and Pfahl et al. experimental data in developing a detailed kinetic mechanism for DME oxidation over wide ranges of temperature and pressure.

In the same time period, Edgar et al. [16] reported constant volume bomb experiments in which DME was injected as a liquid into a hot gaseous inert or oxidizing media. Edgar et al. proposed a general detailed chemical kinetic mechanism to describe the pyrolysis, oxidation and autoignition experiments of DME in a constant volume, premixed mixture. However, the experiments themselves were not sufficiently well defined to permit testing and validation of the proposed mechanism. The DME injection process led to a spatial distribution of fuel/air equivalence ratio within the volume, along with non-homogeneous temperature distributions in the bomb. The kinetic mechanism of Edgar et al. produced qualitative behavior similar to their experimental observations, but the mechanism was not compared with other experimental data present in the literature. The authors propose formic acid as a potential reactive intermediate resulting from low and intermediate oxidative

processes. However, no experimental data were generated to confirm or deny these portions of the proposed mechanism.

The first results from the present experimental studies [6] were reported in early 1997 [17]. Oxidation of DME at high pressures (12.5 atm) and low and intermediate temperatures (490-790 K) confirmed the existence of a negative temperature coefficient regime from 590-690 K, followed by an intermediate temperature regime, ending in hot ignition above 780 K. More importantly, FTIR spectral analyses of the reaction products identified formic acid as significant reaction intermediate at temperatures near 500 K. Although the formic acid was not fully quantified (calibration work had not been completed), its presence suggested that proposed dimethyl ether kinetic mechanisms should include this species as a significant intermediate at low temperatures. Calibrated, quantified data showing that formic acid was indeed a major intermediate found at low and intermediate reaction temperatures, substantially exceeding formaldehyde concentrations, were first presented in 1998 [18].

Recently, Dagaut et al. [2] reported additional experimental studies of DME in their jet-stirred reactor. Data were obtained at 10 atm in the temperature range 500–800 K, using extractive gas sampling and gas chromatography with flame ionization detection. Formaldehyde and hydrocarbon products were identified and quantified, but formic acid was not observed to be a reaction intermediate. In contrast with our results we speculated in comments on the Dagaut et al. paper [2], that formic acid was lost in the analytical measurement apparatus. However, the carbon balances reported in the work suggests that there are no significant concentrations of unidentified species present. Thus, we are at a loss as to why formic acid was not observed, unless it was somehow converted during the sample quenching process to other carbon/hydrogen/oxygen-containing intermediates that were correctly quantified. As a result of their experimental evidence, Dagaut et al. modeled their results using the low temperature portion of the DME mechanism from Curran et al., without modifications in the earlier reaction scheme. Instead, rate expressions were adjusted to gain agreement with the new JSR data. Predictions using this mechanism continue to suggest a minor presence of formic acid as an intermediate at low and intermediate temperatures, consistent with their experimental observations, Figs. 22 and 24.

Finally, Liu et al. [19], have recently reported studies on the oxidation of DME (340 ppm DME in 10% O_2) in an atmospheric pressure, laminar flow reactor, at temperatures from $513 \leq T \leq 973$ K and residence times in the range 2 to 4 seconds. The products leaving the reactor were analysed using Fourier-Transform Infra-Red Spectroscopy. It was found that the products in this low-temperature region included formaldehyde, carbon monoxide and formic acid. Confirming our measurements, formic acid was determined to be a major reaction intermediate in the low temperature oxidation.

The current experimental and modeling collaboration was undertaken to advance prior modeling efforts to be consistent with observations of formic acid as a major intermediate at low and intermediate reaction temperatures. The work extends understanding of dimethyl ether oxidation at low temperatures, i.e. temperatures at which the methoxymethyl radical undergoes addition to molecular oxygen, followed by internal H-atom transfer, a second addition to molecular oxygen and eventual chain-branching. Kinetic measurements obtained in the VPFR were compared to predictions from previously published detailed kinetic mechanisms [1, 2], which did not include a direct pathway for formic acid production from DME, a deficiency immediately apparent in comparisons. A more thorough study of the low tem-

perature mechanism reveals a new pathway for formic acid formation that is logical and that has been overlooked previously. In the course of the modeling studies, we also modified some important rate constant expressions used in prior modeling, in response to more current understanding of thermochemical parameters and rate estimations. Overall, we have obtained good agreement between model simulation and experimental observations in the VPFR. We also find good agreement with the earlier shock tube experiments of Pfahl et al. [3] and the JSR experiments of Dagaut et al. [2], [15] (neglecting comparison of formic acid predictions and the experiments).

Experimental Description

All of the experiments reported here were performed in the Princeton Variable Pressure Flow Reactor (VPFR). The VPFR can access a wide range of conditions: temperature (550-1200 K); pressure (0.3-20 atm); and equivalence ratio (pure pyrolysis to oxygen-rich conditions). The VPFR facility, as well as the sampling and analytical techniques utilized in the present work, are fully described in the companion paper [4]. A sampled flow obtained using a hot-water-cooled, wall-convection-quenched, stainless steel sample probe was analyzed using a Nicolet Model 730 FTIR, equipped with a heated, 0.7 liter, 10 meter multi-reflective cell, with spectral absorbance resolution of 0.125 cm^{-1}. The cell pressure (760 mm Hg) and temperature (100°C) were held constant for all measurements. The analytical flow exiting the cell was then directed to a continuous flow electrochemical analyzer for O_2, to continuous non-dispersive infrared (NDIR) analyzers for CO and CO_2, and to a continuous selective detector for H_2. Each species concentration was determined, with the exceptions of formic acid and water, from spectral features that were isolated from interference produced by other species. Formic acid and water spectra interference could not be completely separated, and a multi-component absorbance calibrations had to be performed for these two species. FTIR species concentration uncertainties were as follows: CH_3OCH_3 (4% or $<$ 50 ppm), CH_4 (2%), CH_3OH (2%), C_2H_6 (2%), C_2H_4 (2%), CH_2O (5% or $<$ 10 ppm), HOCHO (3.5% or $<$ 12 ppm), H_2O (10%). Other analytical measurements had uncertainties as follows: O_2 (3%); CO (2%); CO_2 (2%). No other hydrocarbon species ($>$ 1 ppm) were detected in the experiments reported here or in the companion paper. The reaction temperature at the gas sampling location was measured with a silica coated Pt-13%Rh/Pt thermocouple ($\approx$ 3 K uncetainty). Further details of the apparatus and techniques can also be found elsewhere [6].

Dimethyl ether was studied at equivalence ratios (ϕ) in the range $0.7 \leq \phi \leq 4.2$ with nitrogen diluent of approximately 98.5%. Experiments were performed over an initial reactor temperature range of 550–850 K, in the pressure range 12–18 atm. Four distinct sets of experiments were performed to characterize the low and intermediate temperature oxidation characteristics. The first set of experiments were conducted at a constant fuel/oxidizer ratio of approximately one, at constant pressure and residence time (12.5 atm and 1.8 s, respectively), and with different initial reaction temperatures. The initial reaction temperature of the flow in the reactor was set at a particular value and the entire reactor system, without fuel flow, was allowed to thermally equilibrate. Fuel flow was then commenced and after stabilization of the analytical measurement readings at the sampling location, compositional data were obtained for the sampled flow and the reaction temperature at the sampling location. Fuel flow was then turned off and the initial reactor temperature was incrementally

changed. The axial distance from the fuel vapor injection location to the sampling location was varied so that, for each initial flow temperature, the same reaction residence time was maintained (flow density correction). The entire procedure was then repeated at the new initial reactor temperature. The reaction conditions in the reactor are adiabatic, so the temperature in the flow field from the mixing point (initial reaction temperature) and the sampling location changes, depending on the exothermicity/endothermicity of the reaction. The composite of many such experiments develops profiles of reactant, intermediate, and product species concentration at fixed residence time as a function of the initial reaction temperature (so-called "reactivity" profiles), see Figs. 3 and 4.

Comparison of such profiles with computational modeling results typically requires that both the chemical induction and post-chemical induction phenomena are modeled, i.e., reaction residence time requires the assignment of a "zero" reaction time. This is typically the approach taken by several other investigators utilizing flow reactors, for example, Alzueta et al. [20]. Such comparisons include uncertainties associated with the effects of impurities and mixing on the induction chemistry. These uncertainties cannot be easily accounted for in the modeling comparisons; however, the data obtained are extremely useful in determining the conditions under which low temperature, negative temperature, or intermediate temperature kinetics occur for a given fuel/oxidizer system. In the present work, these data were very useful for setting initial conditions for the remaining three sets of experiments discussed below.

Based upon the reactivity data, three other series of experiments were performed, under fixed equivalence ratio conditions, at a pressure of 12.5 atm, and at various constant initial reaction temperatures. In each experiment, the reaction residence time was changed by moving the position of the mixing location relative to the sampling location. The flow reactor and sampling/analytical systems were allowed to stabilize, and chemical compositional data and sample point temperature were obtained. The mixing location was changed, and the process was repeated. Reactant, intermediate, and product composition and flow reaction temperature were then correlated for fixed initial conditions as a function of reaction residence time.

The second series utilized near-stoichiometric equivalence ratio of DME and oxygen and a number of initial reactant temperatures corresponding to various points in the regime of negative temperature coefficient (NTC) behavior, see Figs. 5–10. A third set of experiments was performed in which the equivalence ratio was varied from lean, through stoichiometric to rich, with product species concentrations correlated against residence time, Figs. 11–16. These experiments were all performed at the same pressure ($\approx$ 12 atm) and at a constant initial reaction temperature of 850 K. The fourth set of experiments depicted the oxidation effects at increasing reaction pressure, at an initial reaction temperature of approximately 590 K, an equivalence ratio of approximately 1.0. In these experiments, reaction pressure was held at 12.5, 17 and 18 atm, see Figs. 5–6 and Figs. 17–20.

Because reaction times between movement of the mixing location are relative to one another, with the same mixing and contaminant perturbations of the induction chemistry, it is more useful to compare the calculated and experimental species- and temperature-time histories by matching them at some intermediate extent of reaction. Further details justifying this method of comparison appear in the companion paper [4].

Computational Model

All of the modeling computations in this study were carried out using the HCT modeling code [21]. The boundary conditions used modeling flow reactor, stirred reactor, and shock tube studies are discussed in the companion paper.

Tables 1 and 2 in the companion paper summarize the detailed kinetic mechanism and theromochemistry used in the calculations shown in both papers. The thermodynamic properties for the relevant radicals and stable parents were obtained by group additivity using THERM [22] with updated H/C/O groups and bond dissociation groups [23]. The thermochemical data, listed in Table 2 of the companion paper, allow the calculation of reverse reaction rate constants by microscopic reversibility. A comparison of our current THERM generated thermochemical values with those recommended by Dagaut et al. [2] and Yamada et al. [24] for a number of selected species are reported in Table 1. We have updated the group values for alkyl-peroxide species based on the recent studies of Yamada et al. [24] and have modified these slightly so that the thermodynamic functions of $\dot{R} + O_2 \rightleftharpoons R\dot{O}_2$ reactions agree with the experimental and calculated values of Knyazev and Slagle [25] for ethyl radical, Table 2. Our chosen heat of formation for the methoxymethyl radical of 1.0 kcal/mol is in good agreement with 0.3 kcal/mol recommended in the NIST structures and properties database, [26] and 0.9 kcal/mol calculated by Good and Francisco [27].

Dimethyl Ether Oxidation Mechanism

The overall reaction scheme for DME oxidation can be depicted as follows:

The species names are defined as follows: CH_3OCH_3 (dimethyl ether), $CH_3O\dot{C}H_2$ (methoxymethyl radical), $CH_3OCH_2\dot{O}_2$ (methoxymethyl-peroxy radical), $\dot{C}H_2OCH_2O_2H$ (hydroperoxymethoxymethyl radical), $\dot{O}_2CH_2OCH_2O_2H$ (peroxy-methoxymethyl-hydroperoxide radical) and HO_2CH_2OCHO (hydroperoxy-methylformate).

At the low temperatures of the present study, the methoxymethyl radical adds to molecular oxygen to form the methoxymethyl-peroxy radical. This adduct can then undergo an intra-molecular H-atom isomerization, and proceed through the relatively complex reaction scheme depicted in Fig. 1. In the temperatures range 550–600 K, chain branching is primarily due to the reaction pathway leading through the carbonyl-hydroperoxide HO_2CH_2OCHO species with the formation of two reactive hydroxyl radicals. As the temperature increases above 600 K, the β-scission of the $\dot{C}H_2OCH_2O_2H$ radical gradually becomes more important. This pathway produces only one reactive hydroxyl radical in addition to two stable molecules of formaldehyde, and thus the overall reactivity of the system decreases leading to a negative temperature coefficient (NTC) region (600–725 K). At initial reactor temperatures above 730 K, H_2O_2 dissociates into two reactive hydroxy radicals leading to a rapid increase in the system's reactivity and consumption of the remaining fuel. DME reacts more exothermically at these temperatures, increasing the temperature above the initial reactor temperature. At low temperatures, H atom abstraction from the fuel occurs primarily by $\dot{O}H$ radicals, reaction (274). (Reaction numbers refer to the number in the reaction mechanism). At higher temperatures (650–750 K) hydroperoxy and methylperoxy radicals also contribute to H atom abstraction, reactions (277) and (278). The rate expressions used here are based on the recommendation of Walker [28] of 2.8×10^{12} exp (-17.7 kcal/RT) cm^3 mol^{-1} s^{-1} per

H atom for the abstraction of secondary H atoms from an alkane by $H\dot{O}_2$ radicals. This results in an $\mathcal{A}$-factor of 1.68×10^{13} using a degeneracy of six. In previous work [1], the $\mathcal{A}$-factors for reactions (277) and (278) were lowered to 1.0×10^{13} in order to obtain better agreement of simulated ignition delay time with the shock tube results of Pfahl et al. [3], particularly at about 1000 K. However, model comparisons with the present flow reactor experiments indicate that faster rate expressions for reactions (277) and (278) are necessary. The comparison of the revised model with the shock tube results of Pfahl et al. can be seen in Fig. 25.

The methoxymethyl radical formed can undergo two different reactions:

- β-scission to yield formaldehyde and methyl radicals.
- addition to molecular oxygen to produce methoxymethyl-peroxy radicals, $CH_3OCH_2\dot{O}_2$.

$$CH_3O\dot{C}H_2 \xrightarrow{282} CH_2O + \dot{C}H_3$$
$$CH_3OCH_2\dot{O}_2 \xleftrightarrow{287} CH_3O\dot{C}H_2 + O_2$$

The rate expression for CH_3OCH_2 β-scission (reaction 282), was taken from Loucks and Laidler [29] and is consistent with the value used in previous work [1]. The bimolecular addition of methoxy-methyl radical to O_2 has no activation energy barrier associated with it. The $\mathcal{A}$-factor for addition to O_2 was taken to be 2.0×10^{12} cm^3 mol^{-1} s^{-1}, that is twice the value used in previously. The high pressure rate expression recommended by Sehested et al. [12] seems to be closer to 6.0×10^{12} cm^3 mol^{-1} s^{-1} at 296 K, a result consistent with this upward revision.

The $CH_3OCH_2\dot{O}_2$ radical formed at low temperatures can undergo three different types of reaction:

1. Decomposition to $CH_3O\dot{C}H_2 + O_2$. This rate constant is the reverse of reaction (287) above, and is calculated from the reverse rate constant and from microscopic reversibility (thermochemistry).

2. Intermolecular abstraction of hydrogen atoms from other hydrocarbon species to produce the stable methoxymethyl-hydroperoxide species, ($CH_3OCH_2O_2H$), which then decomposes to $CH_3OCH_2\dot{O} + OH$, followed by reactions of the $CH_3OCH_2\dot{O}$ radical. Experimental and modeling results showed this sequence of reactions to be of relatively minor importance here.

3. The most important step involves isomerization of the $CH_3OCH_2\dot{O}_2$ radical *via* internal H atom transfer to form hydroperoxy-methoxymethyl radical, $\dot{C}H_2OCH_2O_2H$.

$$CH_3OCH_2\dot{O}_2 \overset{293}{\rightleftharpoons} \dot{C}H_2OCH_2O_2H$$

The estimation of this rate constant is as described in our previous study [1]. We estimate the activation energy, $\mathcal{E}_a$, using the expression,

$$\mathcal{E}_a = \Delta H_{\text{rxn}} + \text{ring strain} + E_{\text{abst}}$$

where $\Delta H_{\rm rxn}$ is taken to be the enthalpy of reaction and is included only if the reaction is endothermic. The activation energy for abstraction is determined, following the analysis of Bozzelli and Pitz [30], from an Evans-Polanyi plot, $E_{\rm abst}$ vs $\Delta H_{\rm rxn}$ (taken in the exothermic direction), of similar H atom abstraction reactions, RH + $\dot{\rm R}'$ = $\dot{\rm R}$ + R′H, leading to the following expression:

$$E_{\rm abst} = 12.7 + (\Delta H_{\rm rxn} \times 0.37)$$

As this transition state involves a six membered ring, we assume a ring strain of 2.3 kcal/mol, similar to our work on n-heptane [31] and neopentane oxidation [32]. In addition, $\Delta H_{\rm rxn} = +10.6$ kcal mol^{-1} and therefore $\mathcal{E}_a = 21.6$ kcal mol^{-1}. The $\mathcal{A}$-factor was chosen to be 6.0×10^{10} s^{-1}, identical to that we now use for a (1,5) transition state ring in our current modeling of n-heptane oxidation. The reverse isomerization rate constant is based on the forward rate constant and on calculated thermodynamic properties using group additivity.

The hydroperoxy-methoxymethyl species formed can react *via* three major pathways.

1. Reverse isomerization of $\dot{\rm C}H_2OCH_2O_2H$ radical (reaction 293) to $CH_3OCH_2\dot{O}_2$ radical as described above.

2. The $\dot{\rm C}H_2OCH_2O_2H$ species can undergo β-scission, leading to the formation of two molecules of formaldehyde and $\dot{\rm O}$H radical, as the hydroperoxy-methyl radical ($\dot{\rm C}H_2O_2H$) is assumed to decompose into formaldehyde and $\dot{\rm O}$H radical very quickly.

$$\dot{\rm C}H_2OCH_2O_2H \overset{294}{\rightleftharpoons} CH_2O + CH_2O + \dot{\rm O}H$$

This endothermic rate constant is unknown but was estimated as follows. The reverse rate (i.e. addition of hydroperoxy-methyl radical to formaldehyde) was likened to a methyl radical adding across the double bond in ethylene to yield the n-propyl radical. The rate for this reaction was taken from Baulch et al. [33] to be 2.1×10^{11} exp (−7.4 kcal/RT) cm^3 mol^{-1} s^{-1}. The forward rate constant expression, calculated by microscopic reversibility was calculated to be 1.5×10^{13} exp (−20.76 kcal/RT) cm^3 mol^{-1} s^{-1}. Previously, it was found that it was necessary to adjust the calculated forward activation energy downward by 3.0 kcal mol^{-1} in order to predict the ignition delay times measured by Pfahl and co-workers [3]; in particular, to simulate the point at which the NTC region comes into effect. However, we find that the low temperature ignition delays of Pfahl et al. can be predicted with the current rate expression, Fig. 25, which depends on the relative rates of alkyl-peroxy radical isomerization and hydroperoxy-alkyl radical addition to molecular oxygen.

3. In addition, hydroperoxy-methoxymethyl species can react with molecular oxygen to form the $\dot{\rm O}_2CH_2OCH_2O_2H$ radical.

$$\dot{\rm O}_2CH_2OCH_2O_2H \overset{295}{\longleftrightarrow} \dot{\rm C}H_2OCH_2O_2H + O_2$$

The reverse rate constant of this reaction was taken to be 7.0×10^{11} cm^3 mol^{-1} s^{-1}. This rate expression was chosen to provide the best agreement with the experimental data, and is approximately 20% lower than the value used previously [1].

It is important to note that the fate of the $\dot{C}H_2OCH_2O_2H$ radical determines the reactivity of the system at low temperatures; a faster rate of β-scission of $\dot{C}H_2OCH_2O_2H$ radical leads to reduced reactivity, while addition to O_2 leads to chain branching and hence greater reactivity.

The $\dot{O}_2CH_2OCH_2O_2H$ radical isomerizes, releasing $\dot{O}H$ and producing a stable carbonyl-hydroperoxide molecule, HO_2CH_2OCHO, Fig. 1.

$$\dot{O}_2CH_2OCH_2O_2H \overset{296}{\rightleftharpoons} HO_2CH_2OCHO + OH$$

The rate for this isomerization *via* an internal H atom transfer, presented in the mechanism is based on the analogous $CH_3OCH_2\dot{O}_2 \rightleftharpoons \dot{C}H_2OCH_2O_2H$ isomerization. The activation energy has been calculated to be 18.6 kcal mol^{-1} (3.0 kcal/mol less than the isomerization of $CH_3OCH_2\dot{O}_2$) and the $\mathcal{A}$-factor has been reduced by two thirds, consistent with the number of H atoms present.

The decomposition of the carbonyl-hydroperoxide molecule leads to chain branching, as two radicals are formed from its decomposition, $\dot{O}H$ and $\dot{O}CH_2OCHO$ radicals.

$$HO_2CH_2OCHO \overset{297}{\longrightarrow} \dot{O}CH_2OCHO + OH$$

Sahetchian et al. [34] published rate constant expressions for the pyrolysis of a number of organic hydroperoxides. Their work indicates a rate expression of about 1.0 $\times 10^{16}$ exp (−43.0 kcal/RT) cm^3 mol^{-1} s^{-1} for a typical RO–OH homolysis reaction. In this study, we have employed a rate expression of 2.0 $\times 10^{16}$ exp (−40.5 kcal/RT) cm^3 mol^{-1} s^{-1}, in order to obtain good agreement with experimental results, particularly at the lowest temperatures. It has been shown in the previous work [1] that shock tube ignition delay times had the highest sensitivity to this reaction at 650 K, with very little sensitivity at higher temperatures.

An important change to the prior mechanism [1] is the fate of the $\dot{O}CH_2OCHO$ radical produced from the decomposition of the carbonyl-hydroperoxide molecule. It was previously assumed that this radical decomposed to produce formaldehyde and a $H\dot{C}O_2$ radical. However, it is also possible for this radical to isomerize *via* an intramolecular H-atom isomerization to form another radical, a process which is exothermic.

$$\dot{O}CH_2OCHO \overset{298}{\longrightarrow} CH_2O + HCO_2$$

$$\dot{O}CH_2OCHO \overset{303}{\rightleftharpoons} HOCH_2O\dot{C}O$$

Based on experimentally measured product yields, we found that the $\dot{O}CH_2OCHO$ radical does undergo β-scission to a small extent but predominantly isomerizes to the $HOCH_2O\dot{C}O$ radical. The rate expression for this isomerization was calculated in the same way as for the methoxymethyl-peroxy radical discussed above. A rate expression of 1.0 $\times 10^{11}$ exp (−14.0 kcal/RT) cm^3 mol^{-1} s^{-1} was estimated. The $HOCH_2O\dot{C}O$ radical is similar to the $HO\dot{C}O$ radical studied by Troe and co-workers [35, 36] and Golden et al. [37, 38], in the reaction sequence $CO + OH = HOCO^\star = CO_2 + H$. The $HOCH_2O\dot{C}O$ radical can decompose *via* two possible pathways:

$$HOCH_2O\dot{C}O \overset{304}{\longrightarrow} HOCH_2\dot{O} + CO$$

$$HOCH_2O\dot{C}O \overset{305}{\longrightarrow} \dot{C}H_2OH + CO_2$$

Figure 2 depicts the reaction coordinate diagram for the $HOCH_2\dot{O}$ + CO = $HOCH_2O\dot{C}O$ = $\dot{C}H_2OH$ + CO_2 system. It is evident that the barrier heights for reactions (304) and (305) are almost identical. Analysis of the $HO\dot{C}O$ system indicates an activation energy of 29 kcal/mol for the addition of H atom to carbon dioxide. Our experience for addition reactions to ethylene indicates an activation energy of 1.2 kcal/mol for H atom addition, with the activation energy increasing to 7.4 kcal/mol for the addition of a methyl radical. Assuming that addition to CO_2 by $\dot{C}H_2OH$ radical is more similar to methyl radical than H atom addition, we estimate an activation energy of (6.2 + 29) = 35.2 kcal/mol for reaction (305). The rate expression for the addition of $HOCH_2\dot{O}$ radical to CO was estimated to be 1.5×10^{11} exp (−4.8 kcal/RT) cm^3 mol^{-1} s^{-1}, similar to that recommended by Tsang and Hampson [39] for ethyl addition to carbon monoxide. The reverse rate for reaction (305) was estimated to be 1.5×10^{11} exp (−35.2 kcal/RT) cm^3 mol^{-1} s^{-1}. These rate expressions result in a sufficiently slow rate of reaction (305) to allow the predominance of reaction (304), the formation of the $HOCH_2\dot{O}$ radical and CO. The $HOCH_2\dot{O}$ radical then decomposes to yield formic acid and H atom. This product channel is necessary to obtain the agreement between simulated and experimental formic acid yield.

Discussion

In this section, the product species concentrations calculated by the model and measured in the experiments are discussed and compared. These experiments are a stringent examination of the low temperature portion of the model, as they test the detailed distribution of both primary and secondary product formation at various temperatures and pressures. Comparisons of the product species profiles measured in the experiment and calculated by the model simulation are shown in Figs. 3–20. It is evident that the predicted concentration profiles for the fuel, oxygen and each product species are in good agreement with the experimental measurements.

Figures 3 and 4 depict experimental and simulated species concentration profiles versus initial reactor temperature at an experimental residence time of 1.8 s. The experimental time is calculated from integration of the axial flow velocity distribution over the distance from the mixing location to the sampling location in the reactor. In Figs. 5 and 6 speciation profiles versus time the simulated profiles had to be time-shifted by −0.3 s relative to the experimental results to achieve comparison of the 50result of modifications of the chemical induction chemistry due to small impurities in the reactants and mixing related effects near the fuel injection location. Thus, the simulation results shown in Figs. 3 and 4 are calculated using a residence time of 2.1 s (rather than 1.8 s) to approximately correct for these same effects on the experimentally measured reactivity profiles. In addition, the reaction conditions are assumed to be adiabatic, and thus the temperature calculated at the sampling location is a result of energetic changes due to reaction and the initial reaction temperature of the calculations themselves.

At low temperatures the primary products formed are carbon monoxide (CO), formic acid (HOCHO), formaldehyde (CH_2O), water (H_2O) and carbon dioxide (CO_2). Methane (CH_4) and ethane (C_2H_6) are also formed at initial reactor temperatures greater than about 730 K.

It is clear from Figs. 3 and 4 that dimethyl ether exhibits NTC behavior experimentally, consistent with that observed in the shock tube results of Pfahl et al. The fuel starts to react

at an initial reactor temperature of 530 K, reaching a maximum reactivity at 593 K. At this temperature, the concentrations of formic acid, carbon monoxide and water peak, with values of 1000, 1340 and 2450 ppm respectively, far greater than the 119 ppm of formaldehyde. This fast rate of oxidation is due to the hydroperoxy-methoxymethyl radical addition to molecular oxygen, subsequent isomerization and chain branching, with the production of formic acid, carbon monoxide, two reactive hydroxyl radicals and one H atom, Fig. 1. Above 600 K, the overall rate of oxidation decreases until the initial reactor temperature reaches 720 K. In this temperature range the concentrations of formic acid, carbon monoxide, and water decrease, while the concentration of formaldehyde gradually increases. This can be explained by the increasing rate of the hydroperoxy-methoxymethyl radical β-scission, reaction (294), to form two formaldehyde molecules and one hydroxyl radical. This reaction is chain propagating, competing with the chain branching reaction, thus decreasing the overall oxidation rate.

At temperatures above 720 K, the overall rate of reaction starts to increase again. When the initial reactor temperature reaches about 750 K, the partial reaction of DME is great enough to raise the reactor temperature above the threshold temperature for hydrogen peroxide decomposition, leading to the formation of two reactive hydroxyl radicals and the observed rapid increase in overall reactivity. At these higher temperatures, β-scission of the alkyl radical becomes important, leading to the formation of methyl radicals and accounting for the formation of methane and ethane. The methyl radicals formed react with hydroperoxy radicals, leading to the formation of methoxy and hydroxy radicals $\dot{C}H_3 + H\dot{O}_2 = CH_3\dot{O} + \dot{O}H$ followed by $CH_3\dot{O} + M = CH_2O + \dot{H} + M$, a process which is chain branching. The formaldehyde produced undergoes further reaction, primarily *via* $CH_2O + \dot{R} = H\dot{C}O + RH$ and $H\dot{C}O + O_2 = CO + H\dot{O}_2$. In the temperature range 750–775 K the measured concentration of formic acid increases again and then becomes almost insignificant at 800 K, while the concentration of formaldehyde gradually decreases from 740–800 K.

Overall, there is good agreement between the model and experiment. However, there are some discrepancies that should be addressed. At 553 K the experiment indicates that almost 19% of DME fuel has reacted although the model predicts only about 5% conversion. The model is slow to react as the activation energy for the carbonyl-hydroperoxide species is quite high (41–43 kcal/mol). As stated earlier, we increased the rate of the carbonyl-hydroperoxide decomposition reaction in order to improve agreement at these low temperatures. At higher temperatures, the rapid increase in reactivity is observed experimentally to start at 730 K, but the model predicts a slower rate of reaction, the rapid increase in reactivity starting about ten degrees higher at 740 K. As observed in the sensitivity analysis the fuel is particularly sensitive to H atom abstraction by $H\dot{O}_2$ and $CH_3\dot{O}_2$ radicals in this temperature range. Subsequently, hydrogen peroxide forms two reactive hydroxyl radicals and methyl peroxide generates methoxy and hydroxyl radicals.

Figures 5–10 show species evolution versus residence time at chosen inlet temperatures, corresponding to various points along the NTC curve. These experiments were performed under near-stoichiometric conditions and at a pressure of 12.5 atm. Figures 5 and 6 show the results at 593 K where the modeling data have been offset by -0.3 s, while the data at 650 K and 710 K did not need to be offset, Figs. 7–10. At 593 K the model shows a little more reactivity than that observed in the experiment. The model-predicted temperature profile is about 10 K higher than that observed in the experiment. In addition, the CH_2O profile is overpredicted by about a factor of three. However, the formic acid, water, carbon

monoxide and carbon dioxide are all in good agreement with the experimental results. At 650 K the overall between experiment and model is better than at 593 K. At 710 K (Fig. 9), the model predicts very well the DME consumption. The predicted water profile (which is a good indication of the quantity of hydroxyl radical in the system) is under-predicted as are the concentrations of the other primary products, Fig. 10.

The influence of equivalence ratio on DME oxidation has also been investigated, at a pressure of 12 atm and at an average temperature of 850 K. The equivalence ratio varied from lean ($\phi = 0.81$), Figs. 11 and 12 through near-stoichiometric ($\phi = 1.17$), Figs. 13 and 14, to rich ($\phi = 2.48$), Figs. 15 and 16. Product species concentrations are correlated against residence time. As the equivalence ratio is increased from 0.81 to 2.41, the methane and ethane yields increase. The formaldehyde yield peaks at an equivalence ratio of 1.17. As the equivalence ratio is increased from 1.17 to 2.41, the fuel oxidation rate slows, and the overall reaction becomes less exothermic. Overall, we believe that there is good agreement between simulation and experiment. The peak heights and the shape of each species profile match one another quite well. However, in simulating these three experiments, the data had to be offset in order to overlap with the experimentally measured product profiles. Under lean conditions for example, in order to match the measured peaks in the formaldehyde and methane profiles it was necessary to offest the prediction profiles by -0.4 s, Figs. 11 and 12. In so doing, the simulation profiles match fairly well the measured fuel, oxygen, carbon monoxide and water profiles.

Finally, Figs. 5 and 6 and 17–20 show the effect upon oxidation of increasing the pressure, at a temperature of approximately 590 K, an equivalence ratio of approximately 1.0 and at pressures of 12.5, 17 and 18 atm. Product species concentrations are correlated against residence time. No significant change in the profiles over this pressure range was observed. The overall agreement between predictions and experiment is similar to that achieved at the lower pressure conditions.

Shock Tube Comparison

The chemical kinetic mechanism developed here was used to simulate the experimental results of Pfahl et al. [3] in a high pressure shock tube. A comparison of the current model prediction with the experimental results can be seen in Fig. 25. There is good agreement between simulation and experiment. However, the model under-predicts the overall rate of fuel oxidation at lower temperatures, resulting in longer than measured total, and cool flame ignition delay times. In addition, the model predicts a faster than observed ignition at about 1000 K, due primarily to the ignition delay sensitivity to reactions of the fuel with hydroperoxy, reaction (277), and methylperoxy radicals, reaction (278), at this temperature. As discussed earlier, we increased the rate expressions of these reactions to achieve good agreement with the current flow reactor data.

Stirred Reactor Comparison

Finally, we have simulated again the recently published experimental results of Dagaut et al. [2], but with the revised mechanism presented here. These data were taken in a jet-stirred reactor in the temperature range 550–800 K, with 0.2% DME at equivalence ratios of 0.2 and 1.0, at a pressure of 10 atm, and a constant residence time of 1.0 s. Overall

there is good agreement between model and experiment. However, at an equivalence ratio of 1.0 the model predicts more reactivity than observed in the experiment, Figs. 21–24. The revised mechanism overpredicts the concentration of carbon monoxide formed but is in good agreement with experimentally observed formaldehyde and carbon dioxide profiles. In addition, we show predicted formic acid profiles, Figs. 22 and 24, even though this species was not reported by Dagaut and co-workers. Formic acid is predicted to be a major species present in the experiment, containing considerable amounts of the total carbon present in intermediates and reaction products.

Formic Acid Formation

As stated earlier, our previous mechanism did not contain any formic acid chemistry. However, the high yield of formic acid observed in these flow reactor experiments at low temperatures prompted us to perform an analysis of possible theoretical formation pathways. Earlier work [1] proposed that the $\dot{O}CH_2OCHO$ radical decomposed to form formaldehyde and $HC\dot{O}_2$ radical, which decomposed to form carbon dioxide and hydrogen atom. If it is assumed that the $HC\dot{O}_2$ radical does not decompose but reacts with hydrogen peroxide or hydroperoxyl radical to yield formic acid, concentrations of formic acid and formaldehyde of nearly the same order would be expected. This assumption cannot be correct because at 593 K, the point of highest reactivity at low temperatures, the observed concentration of formic acid is almost an order of magnitude greater than that of formaldehyde, Fig. 4.

We suggest, however, that there are two main pathways contributing to formic acid formation. The first is through the $\dot{O}CH_2OCHO$ radical, created from the decomposition of the dimethyl ether carbonyl-hydroperoxide molecule, which is produced directly from one fuel molecule. The $\dot{O}CH_2OCHO$ radical undergoes an internal H-atom shift and generates the $HOCH_2O\dot{C}O$ radical which decomposes to form the $HOCH_2\dot{O}$ radical and CO. The $HOCH_2\dot{O}$ radical produces HOCHO (formic acid) and a H atom. The fact that the experimental concentrations of formic acid and carbon monoxide are very similar in the temperature range 500–600 K lends additional support to this proposed pathway.

The second route to formic acid formation that we propose also involves the $HOCH_2\dot{O}$ radical, but results from the addition of hydroxyl radical to formaldehyde, reaction (307). This pathway is somewhat controversial, as Niki et al. [40] studied the reaction of hydroxyl radicals with formaldehyde at a temperature of 299 K and at a pressure of 700 Torr and found that formaldehyde exclusively undergoes abstraction rather than addition. However, as pointed out by Stief et al. [41] pressure dependence in $k(\dot{O}H + CH_2O)$ may be expected, since the addition reaction is likely to proceed via a chemically activated adduct. We have employed a rate expression of 4.5×10^{15} $T^{-1.1}$ cm^3 mol^{-1} s^{-1} for reaction (307). This rate is based on the recommendation of Taylor et al. [42] for the addition of hydroxyl radical to acetaldehyde, who recommend a high-pressure limit rate coefficient of 3.0×10^{15} $T^{-1.1}$ cm^3 mol^{-1} s^{-1}. Analysis of HCT output edits indicates that at 560 K, the $HOCH_2\dot{O}$ radical is predominantly produced from the decomposition of the $HOCH_2O\dot{C}O$ radical rather than the $\dot{O}H$ addition to CH_2O in the ratio of 6.5:1. The importance of the route through formaldehyde increases steadily, and at a temperature of 660 K its contribution to the formation of formic acid is equal to the direct route from dimethyl ether. Our analysis is supported by experiment because from 600–750 K there is a profound decrease in the concentration of formic acid. However, from 750–775 K the concentration of formic acid is measured to increase again,

as predicted by the HCT simulation. This increase is due to the increased concentration of hydroxyl radicals, formed from the decomposition of hydrogen peroxide, which add to formaldehyde and produce formic acid and hydrogen atom.

This type of reaction has implications too in the oxidation of acetaldehyde, or any other aldehydic species. It may be possible in the case of acetaldehyde, for example, for the hydroxyl radical to add to the aldehydic carbon atom, according to the Fig. 26, producing formic acid and a methyl radical, or acetic acid and a hydrogen atom.

We also investigated the importance of the addition of hydroperoxyl radical to formaldehyde, reaction (-325), and the reaction of hydroperoxyl radical with hydroxymethyl ($\dot{C}H_2OH$) radical, reaction (306).

$$HO_2CH_2\dot{O} \xrightarrow{325} H\dot{O}_2 + CH_2O$$

$$\dot{C}H_2OH + H\dot{O}_2 \xrightarrow{306} HOCH_2\dot{O} + \dot{O}H$$

Analysis of HCT edits indicate that reaction (325) does not contribute to the oxidation of formaldehyde, and reaction (306) does not contribute to the formation of formic acid.

We also considered an alternative route to the decomposition of the carbonyl-hydroperoxide species, HO_2CH_2OCHO, depicted in Fig. 27. This route has also been suggested by Marinov [43], and is presently being further investigated by him. We estimate that the transition state through this system has an energy barrier of about 40–45 kcal/mol. However, the $\mathcal{A}$-factor is about two orders of magnitude lower than that for the decomposition to carbonyl-alkoxy radical and a hydroxyl radical. Thus, we believe that this reaction channel cannot successfully compete with that of the O–O homolysis, reaction (297).

Sensitivity Analysis

A sensitivity analysis was performed by multiplying the rate constant of a reaction by a factor of two (both forward and reverse rate constants) and then calculating the percent change in fuel conversion. Three different temperatures were chosen (593, 650 and 750 K) in order to indicate sensitivity of each reaction to the onset, middle and end of the NTC region at an average pressure of 12.5 atm. Fuel conversion is a good measure of overall reactivity, and hence we define the sensitivity coefficient as the change in fuel conversion compared with the baseline simulation, and express this as a percentage. A positive sensitivity coefficient indicates an increase in the amount of fuel consumed, while a negative sensitivity coefficient indicates a decreased level of fuel conversion. The reaction rate constants that exhibited the highest sensitivity are shown in Fig. 28. Reactions in which we multiplied both forward and reverse rate constants by a factor of two are denoted with an equal to "=" sign between reactants and products and reactions in which we multiplied only the forward rate constant (i.e. effected a change in the equilibrium constant) are denoted with an arrow "⇒" between reactants and products.

At all temperatures the reaction with one of the largest positive sensitivities (most effective in promoting the overall rate of oxidation) is the addition of the hydroperoxymethoxymethyl radical to molecular oxygen:

$$\dot{O}_2CH_2OCH_2O_2H \xleftrightarrow{295} \dot{C}H_2OCH_2O_2H + O_2$$

At low temperatures isomerization of the $\dot{O}_2CH_2OCH_2O_2H$ radical (reaction 296), leads to the formation of the carbonyl-hydroperoxide molecule, HO_2CH_2OCHO, and a hydroxyl radical. Subsequent decomposition of the carbonyl-hydroperoxide molecule leads to the formation of another hydroxyl radical and an oxygenated-alkoxy radical, a sequence which produces a total of three radicals (two of which are reactive hydroxyl radicals) and is, therefore, chain branching. It is interesting to note that this reaction appears to be sensitive only to the radical addition to molecular oxygen (forward rate constant) and not the reverse rate constant. The sensitivity coefficients associated with changing both the forward and reverse rate constants by a factor of two are almost identical to those in which we effected a change only in the forward rate constant at all temperatures.

The reactions that are next greatest in promoting the rate of fuel oxidation are those involving abstraction of hydrogen atoms from the fuel by $\dot{O}H$, $\dot{H}$, $H\dot{O}_2$, and $CH_3\dot{O}_2$:

$$CH_3OCH_3 + \dot{O}H \xrightarrow{274} CH_3O\dot{C}H_2 + H_2O$$

$$CH_3OCH_3 + \dot{H} \xrightarrow{275} CH_3O\dot{C}H_2 + H_2$$

$$CH_3OCH_3 + H\dot{O}_2 \xrightarrow{277} CH_3O\dot{C}H_2 + H_2O_2$$

$$CH_3OCH_3 + CH_3\dot{O}_2 \xrightarrow{278} CH_3O\dot{C}H_2 + CH_3O_2H$$

The sensitivity coefficients pertaining to these reactions increase with increasing reaction temperature, but the effect is more pronounced for abstractions by $H\dot{O}_2$ and $CH_3\dot{O}_2$ radicals, Fig. 28. The concentration of both of these radicals steadily increase with increasing reaction temperature and, at an initial reactor temperature of about 750 K, the H_2O_2 and CH_3O_2H molecules produced decompose more readily to produces reactive hydroxyl and methoxy radicals, reactions (51) and (191).

$$H_2O_2 + M \xrightarrow{51} \dot{O}H + \dot{O}H + M$$

$$CH_3O_2H \xrightarrow{191} CH_3\dot{O} + \dot{O}H$$

$$CH_3OCH_2\dot{O}_2 \overset{293}{\rightleftharpoons} \dot{C}H_2OCH_2O_2H$$

Indeed, reaction (51) shows a very high positive sensitivity at 750 K, Fig. 28.

Adjusting the equilibrium of the methoxymethyl-peroxyl radical isomerization to hydroperoxy-methoxymethyl radical also promotes fuel oxidation, reaction (293). At all temperatures, this leads to the formation of hydroxyl radicals, which abstract hydrogen atoms from the fuel, thus leading to increased reactivity.

The reaction that shows the largest negative sensitivity (most effective in decreasing the overall reactivity at all temperatures) is the β-scission of the hydroperoxy-methoxymethyl radical, reaction (294).

$$\dot{C}H_2OCH_2O_2H \overset{294}{\rightleftharpoons} CH_2O + CH_2O + \dot{O}H$$

As indicated earlier, this reaction generates just one hydroxyl radical and inhibits the addition of hydroperoxy-methoxymethyl radical to molecular oxygen, a reaction that leads to the formation of two reactive hydroxyl radicals and chain branching.

Another reaction which shows a negative sensitivity is the abstraction of H atoms from formaldehyde by hydroxyl radicals, reaction (32).

$$\begin{aligned} CH_2O + \dot{O}H &\xrightarrow{32} H\dot{C}O + H_2O \\ H\dot{O}_2 + M &\xrightarrow{26} \dot{H} + O_2 + M \end{aligned}$$

This reaction competes with abstraction by hydroxyl radicals from the fuel and thus inhibits the overall reactivity of the system. Another reaction that produces similar behavior is the addition of H atoms to molecular oxygen, reaction (-26). This reaction competes with abstraction of H atoms from the fuel by H atoms.

The self-reactions of hydroperoxyl radicals show negative sensitivity coefficients at all temperatures, with the largest values occurring at 750 K. The self reaction results in the formation of only one molecule of hydrogen peroxide. However, reaction of hydroperoxyl radical with the fuel or formaldehyde would result in two molecules of hydrogen peroxide and ultimately *four* hydroxyl radicals.

$$\begin{aligned} H\dot{O}_2 + H\dot{O}_2 &\xrightarrow{50,187} H_2O_2 + O_2 \\ CH_2O + H\dot{O}_2 &\xrightarrow{54} H\dot{C}O + H_2O_2 \end{aligned}$$

Sensitivity to β-scission of the methoxymethyl radical (reaction 282):

$$CH_3O\dot{C}H_2 \xrightarrow{282} CH_2O + \dot{C}H_3$$

shows a negative sensitivity coefficient at 750 K. This reaction competes with the addition of $CH_3O\dot{C}H_2$ radical to O_2 which results in the generation from the $\dot{C}H_2OCH_2O_2H$ radical of a hydroxyl radical which is more reactive than a methyl radical.

Finally, at 750 K the system shows sensitivity to the reaction of methyl and hydroperoxyl radical, reactions (22) and (45). Reaction (22) shows a positive sensitivity as it produces two reactive (methoxy and hydroxyl) radicals, while reaction (45) is inhibiting as it generates two unreactive molecules, namely methane and oxygen.

$$\begin{aligned} \dot{C}H_3 + H\dot{O}_2 &\xrightarrow{22} CH_3\dot{O} + \dot{O}H \\ \dot{C}H_3 + H\dot{O}_2 &\xrightarrow{45} CH_4 + O_2 \end{aligned}$$

Conclusions

The oxidation of DME has been studied in a variable-pressure flow reactor, in the temperature range $550 \leq T \leq 855$ K, in the pressure range $12 \leq P \leq 18$ atm with the equivalence ratio (ϕ) varying from $0.7 \leq \phi \leq 4.2$. It was found that dimethyl ether does exhibit negative temperature coefficient (NTC) behavior, in agreement with the shock tube results of Pfahl et al. These experiments found that formic acid is a major product of the low temperature oxidation of dimethyl ether, consistent with the results presented by Liu et al. [19]. A detailed chemical kinetic mechanism has been used to simulate these experimental results and

overall, there is good agreement between the model and experiment. Two pathways leading to the formation of formic acid have been proposed and are supported by experimental observation.

Previously, we estimated the activation energy of hydroperoxy-methoxymethyl radical β-scission based on that measured by Loucks and Laidler [29] for methoxymethyl radical β-scission but we had to reduce the activation energy for the hydroperoxy-methoxymethyl radical β-scission in order to reproduce the experimental results of Pfahl et al. [1]. Here, we are able to employ an activation energy for hydroperoxy-methoxymethyl radical β-scission consistent with that for the methoxymethyl radical and still achieve satisfactory agreement with experiment.

Concentration profiles of reactants, intermediates and products of the oxidation of DME measured in a JSR [2] at 10 atm, an equivalence ratio of 1.0, in the temperature range 550–800 K, have shown that the model can reasonably predict both primary and secondary product formation. The detailed model was also used to simulate the shock tube experiments of Pfahl et al. [3] for stoichiometric mixtures of DME in air, at temperatures of 650–1300 K and reflected shock pressures of 13–40 bar. It was found that the model was able to predict accurately total ignition delay times and the trends in the first stage or "cool-flame" ignition times. The good agreement found between experimental and modeling predictions under JSR and shock tube conditions gives us added confidence in the reliability of the reaction mechanism, and further evidence of an experimental aberration in the failure to observe formic acid in earlier JSR experiments.

Acknowledgement

The experimental work discussed in this paper and computational work appearing in the thesis of S. Fischer, were conducted at Princeton University. The U.S. Department of Energy, Chemical Sciences Division, Office of Basic Energy Sciences, supported these contributions, and those of Prof. Dryer, under Contract No. DE-FG02-86ER-13503. S. Fischer also wishes to acknowledge the support of her thesis research under the National Defense Fellowship Program. Mr. Paul Michniewicz, Mrs. Yolanda Stein and Dr. Steve Klotz are acknowledged for their assistance in completing the experimental portions of the work. The authors wish to thank Dr. W. J. Pitz and Dr. C. K. Westbrook for their comments and discussions in the preparation of this manuscript. The computations appearing in this paper and the contributions of Dr. Curran were performed under the auspices of the U.S. Department of Energy by the Lawrence Livermore National Laboratory under contract No. W–7405–ENG–48.

References

[1] H. J. Curran, W. J. Pitz, C. K. Westbrook, P. Dagaut, J-C. Boettner and M. Cathonnet, *Int. J. Chem. Kinet.* 30:229–241, (1998).

[2] P. Dagaut, C. Daly, J. M. Simmie and M. Cathonnet, *Twenty-Seventh Symposium (International) on Combustion.*, The Combustion Institute, Pittsburgh, 1998, pp. 361–369.

[3] U. Pfahl, K. Fieweger and G. Adomeit, *Twenty-Sixth Symposium (International) on Combustion.*, The Combustion Institute, Pittsburgh, 1996, 781–789.

[4] H. J. Curran, W. J. Pitz, C. K. Westbrook, S. L. Fischer, F. L. Dryer, *Int. J. Chem. Kinet.* submitted, (1999).

[5] A. M. Rouhi, *Chem. and Eng. News.* pp. 37–39, May 29, (1995).

[6] S. L. Fischer, M.S.E. Thesis, Department of Mechanical and Aerospace Engineering, Princeton University, Princeton, NJ, January, 1999. MAE 3035-T.

[7] T. J. Wallington, M. D. Hurley, J. C. Ball, and M. E. Jenkin, *Chem. Phys. Letters.* 211:41–47, (1993).

[8] M. E. Jenkin, G. D. Hayman, T. J. Wallington, R. D. Hurley, J. C. Ball, O. J. Nielsen and T. Ellermann, *J. Phys. Chem.* 97:11712–11723, (1993).

[9] S. Langer, E. Ljungström, T. Ellermann, O. J. Nielsen and J. Sehested, *Chem. Phys. Letters.* 240:53–56, (1995).

[10] J. Sehested, K. Sehested, J. Platz, H. Egsgaard and O. J. Nielsen, *Int. J. Chem. Kinet.* 29:627–636, (1997).

[11] A. Masaki, S. Tsunashima and N. Washida, *J. Phys. Chem.* 99:13126, (1995).

[12] J. Sehested, T. Møgelberg, T. J. Wallington, E. W. Kaiser and O. J. Nielsen, *J. Phys. Chem.* 100:17218–17225, (1996).

[13] K. Hoyermann and F. Nacke, *Twenty-Sixth Symposium (International) on Combustion.*, The Combustion Institute, Pittsburgh, 1996, 505–512.

[14] M. M. Maricq, J. J. Szente and J. D. Hybl, *J. Phys. Chem.* A 101:5155–5167, (1997).

[15] P. Dagaut, J-C. Boettner and M. Cathonnet, *Twenty-Sixth Symposium (International) on Combustion.*, The Combustion Institute, Pittsburgh, 1996, pp. 627–632.

[16] B. L. Edgar, R. W. Dibble and D. W. Naegeli, Society of Automotive Engineers publication SAE–971677 (1997).

[17] F. L. Dryer and R. A. Yetter, We need to get the proper reference.

[18] F. L. Dryer, Symposium on Kinetics of Combustion Processes, American Chemical Society National Meeting, Dallas, March 27-April 2, 1998, Paper 401.

[19] I. Liu, N. W. Cant, J. H. Bromly, F. J. Barnes, P. F. Nelson and B. S. Haynes, *Twenty-Seventh Symposium (International) on Combustion.*, The Combustion Institute, Pittsburgh, 1998, work in progress poster W1F07.

[20] M. U. Alzueta, J. Muro, R. Bilbao and P. Glarborg, *Israel J. Chem.* 39:73–86 (1999).

[21] C. M. Lund and L. Chase, "HCT - A General Computer Program for Calculating Time-Dependent Phenomena Involving One-Dimensional Hydrodynamics, Transport, and Detailed Chemical Kinetics," Lawrence Livermore National Laboratory report UCRL-52504, revised (1995).

[22] E. R. Ritter and J. W. Bozzelli, *Int. J. Chem. Kinet.* 23:767 (1991).

[23] T. Lay, J. W. Bozzelli, A. M. Dean and E. R. Ritter, *J. Phys. Chem.* 99:14514, (1995).

[24] T. Yamada, W. J. Bozzelli and T. Lay, *Twenty-Seventh Symposium (International) on Combustion*, Combustion Institute, Pittsburgh, 1998, pp. 201–209.

[25] V. D. Knyazev and I. R. Slagle, *J. Phys. Chem. A* 102:1770–1778 (1998).

[26] S. E. Stein, S. G. Lias, J. F. Liebman, R. D. Levin and S. A. Kafafi, NIST Standard Reference Database 25: NIST Structures and Properties Version 2.0, 1994.

[27] D. A. Good and J. S. Francisco, *Chem. Phys. Lett.* 266:512–514 (1997).

[28] R. W. Walker, *Twenty Second Symposium (International) on Combustion*, Combustion Institute, Pittsburgh, 1988, pp. 883–892.

[29] L. F. Loucks and K. J. Laidler, *Can. J. Chem.* 45:2767–2773 (1967).

[30] J. W. Bozzelli, and W. J. Pitz, *Twenty Fifth Symposium (International) on Combustion*, Combustion Institute, Pittsburgh, 1994, p. 783.

[31] H. J. Curran, P. Gaffuri, W. J. Pitz and C. K. Westbrook, *Combust. Flame* 114:149–177 (1998).

[32] S. Wang, D. L. Miller, N. P. Cernansky, H. J. Curran, W. J. Pitz and C. K. Westbrook, *Combust. Flame* 118:415–430 (1999).

[33] D. L. Baulch, C. J. Cobos, R. A. Cox, C. Esser, P. Frank, Th.Just, J. A. Kerr, M. J. Pilling, J. Troe, R. W. Walker and J. Warnatz, *J. Phys. Chem. Ref. Data* 21:411–429 (1992).

[34] K. A. Sahetchian, R. Rigny, J. T. De Maleissye, L. Batt, M. Anwar-Khan and S. Mathews, *Twenty-Fourth Symposium (International) on Combustion*, The Combustion Institute, Pittsburgh, 1992, pp. 637–643.

[35] D. Fulle, H. F. Hamann, H. Hippler and J. Troe, *J. Chem. Phys.* 105:983–1000 (1996).

[36] J. Troe, *Twenty-Seventh Symposium (International) on Combustion*, The Combustion Institute, Pittsburgh, 1998, pp. 167–175.

[37] C. W. Larson, P. H. Stewart and D. M. Golden, *Int. J. Chem. Kinet.* 20:27–40 (1988).

[38] D. M. Golden, G. P. Smith, A. B. McEwen, C.-L. Yu, B. Eiteneer, M. Frenklach, G. L. Vaghjiani, A. R. Ravishankara and F. P. Tully, *J. Phys. Chem.* A 102:8598–8606 (1998).

[39] W. Tsang and R. F. Hampson, *J. Phys. Chem. Ref. Data* 15:1087–1279 (1986).

[40] H. Niki, P. D. Maker, C. M. Savage and L. P. Breitenbach, *J. Phys. Chem.* 88:5342–5344 (1984).

[41] L. J. Stief, D. F. Nava, W. A. Payne and J. V. Michael, *J. Chem. Phys.* 73:2254 (1980).

[42] P. H. Taylor, M. S. Rahman, M. Arif, B. Dellinger and P. Marshall, *Twenty-Sixth Symposium (International) on Combustion*, Combustion Institute, Pittsburgh, 1996, pp. 497–504.

[43] N. M. Marinov, Personal Communication, 1999.

Species	H_f° @ 298 K (kcal/mol)			S_f° @ 298 K (cal/mol-K)		
	[15]	[24]	this study	[15]	[24]	this study
CH_3OCH_3	—	-44.0	-43.4	—	—	63.8
$CH_3O\dot{C}H_2$	-2.0	0.1	1.0	67.4	67.7	67.3
$CH_3OCH_2O_2H$	—	—	-68.4	—	—	83.8
$CH_3OCH_2\dot{O}_2$	—	-33.9	-34.6	—	83.1	82.6
$\dot{C}H_2OCH_2O_2H$	—	-26.5	-24.0	—	88.0	85.9
$\dot{O}_2CH_2OCH_2O_2H$	—	—	-59.6	—	—	101.2

Table 1: Comparison of thermodynamic properties for selected species

Citation	$-\Delta H^\circ_{rxn}$ @ 298 K (kcal/mol)		$-\Delta S^\circ_{rxn}$ @ 298 K (cal/mol-K)	
	$CH_3O\dot{C}H_2$	$\dot{C}H_2OCH_2O_2H$	$CH_3O\dot{C}H_2$	$\dot{C}H_2OCH_2O_2H$
[2]	33.7	32.4	39.0	38.7
[24]	34.0	—	33.6	—
[25]†	35.5	—	33.6	—
this study	35.6	35.6	33.7	33.7

Table 2: Comparison of thermodynamic functions $\dot{R} + O_2 \rightleftharpoons R\dot{O}_2$ reactions. † Kynazev and Slagle number corresponds to ethyl radical.

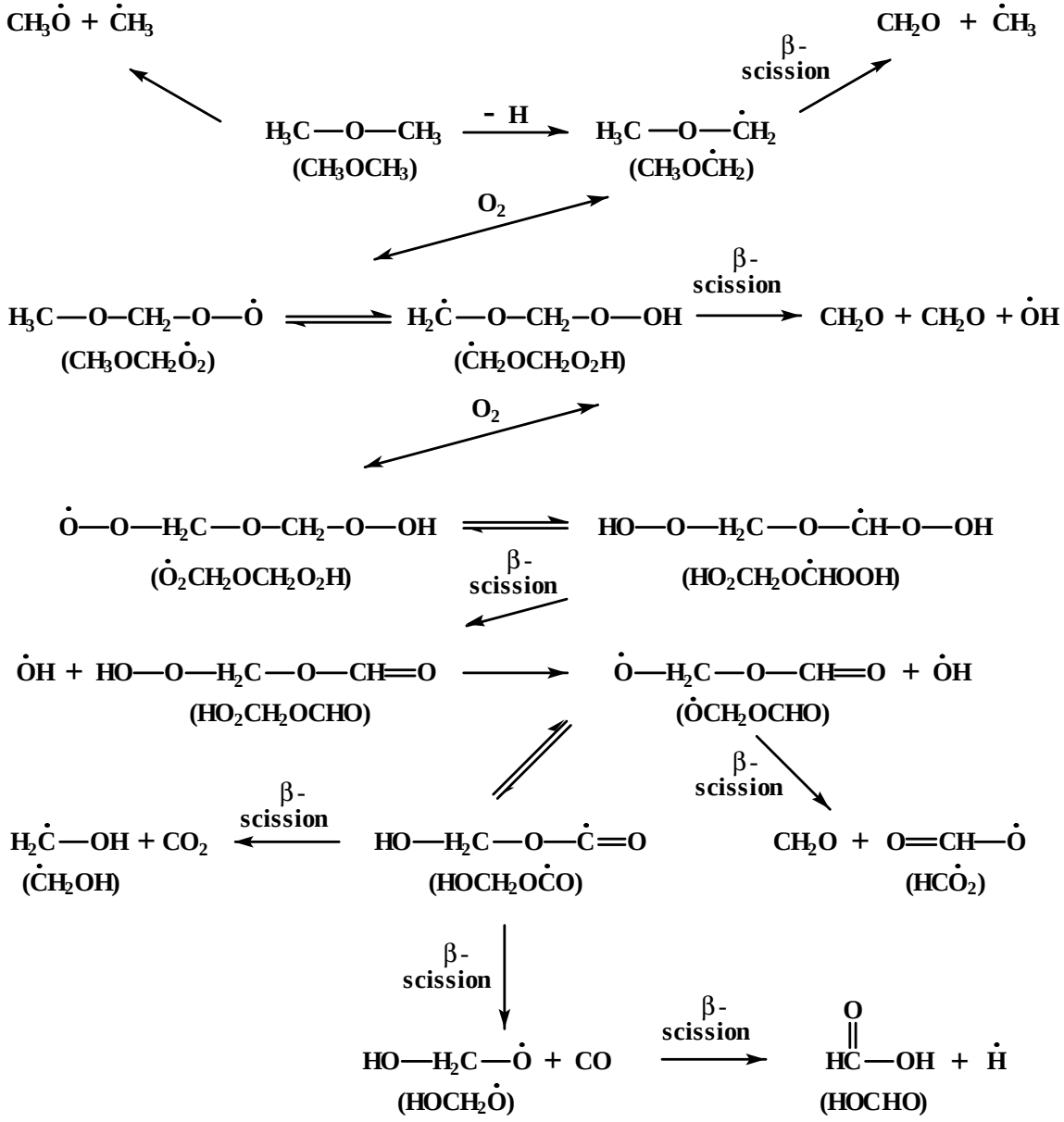

Figure 1: Overall reaction scheme for dimethyl ether oxidation

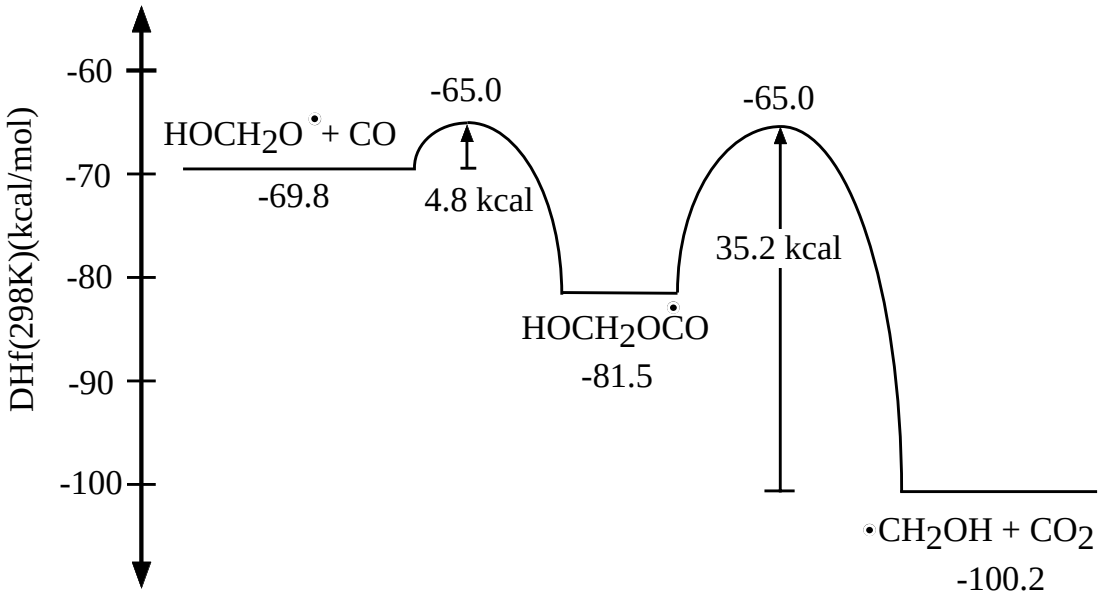

Figure 2: Reaction coordinate diagram for the $HOCH_2\dot{O}$ + CO = $HOCH_2O\dot{C}O$ = $\dot{C}H_2OH$ + CO_2 system.

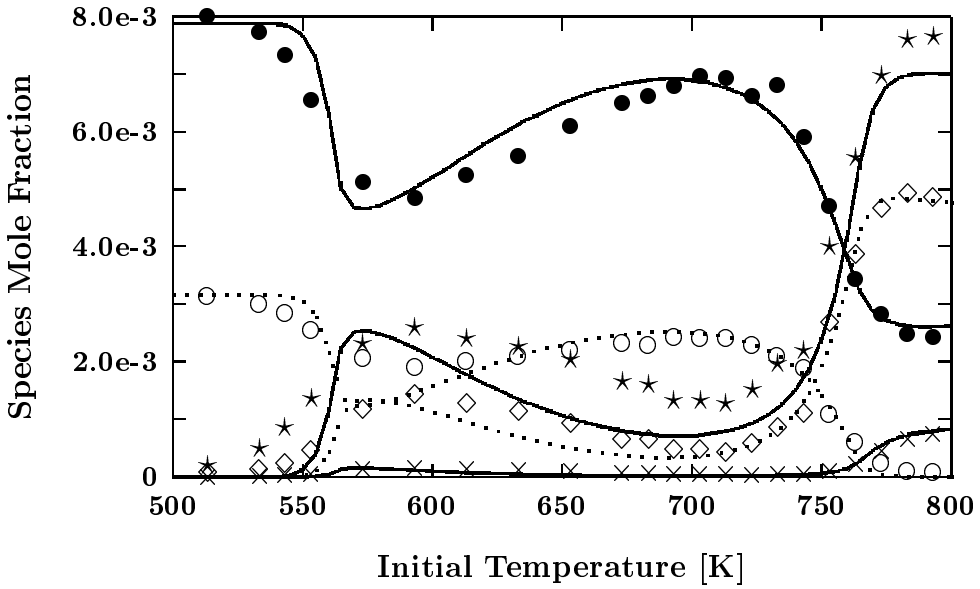

Figure 3: Measured (symbols) and calculated (curves) species concentrations from a flow reactor. 3030 ppm DME, $\phi = 1.19$, P=12.5 atm, τ=1.8 s. $\bullet$ O_2, $\circ$ CH_3OCH_3, $\star$ H_2O, $\diamond$ CO, and $\times$ CO_2. Dotted lines correspond to open symbols.

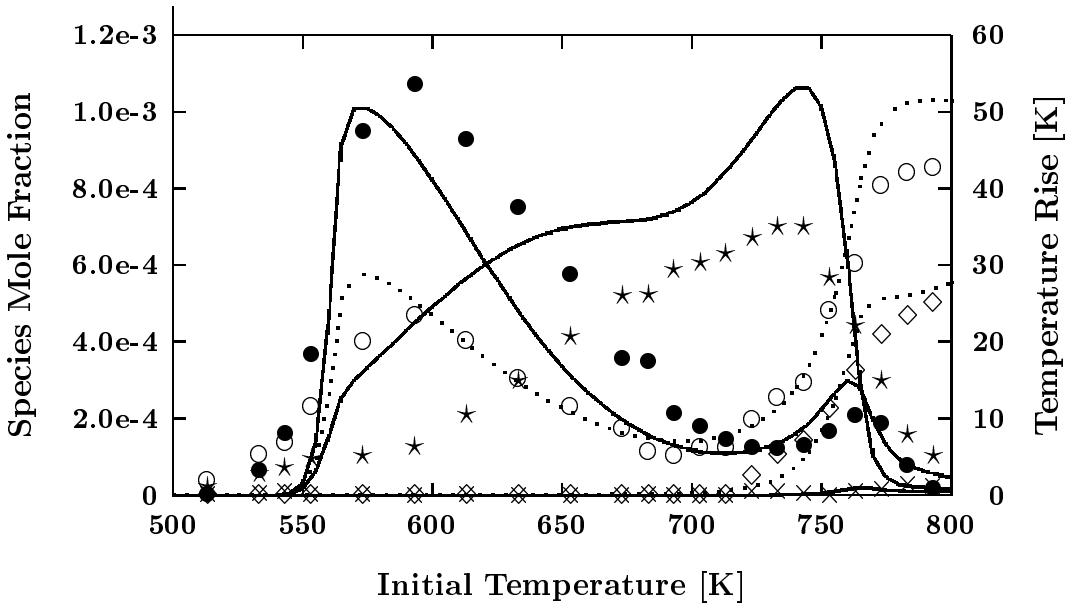

Figure 4: Measured (symbols) and calculated (curves) species concentrations from a flow reactor. 3030 ppm DME, $\phi = 1.19$, P=12.5 atm, τ=1.8 s. $\bullet$ HOCHO, $\circ$ Temperature rise, $\star$ CH_2O, $\diamond$ CH_4, and $\times$ C_2H_6. Dotted lines correspond to open symbols.

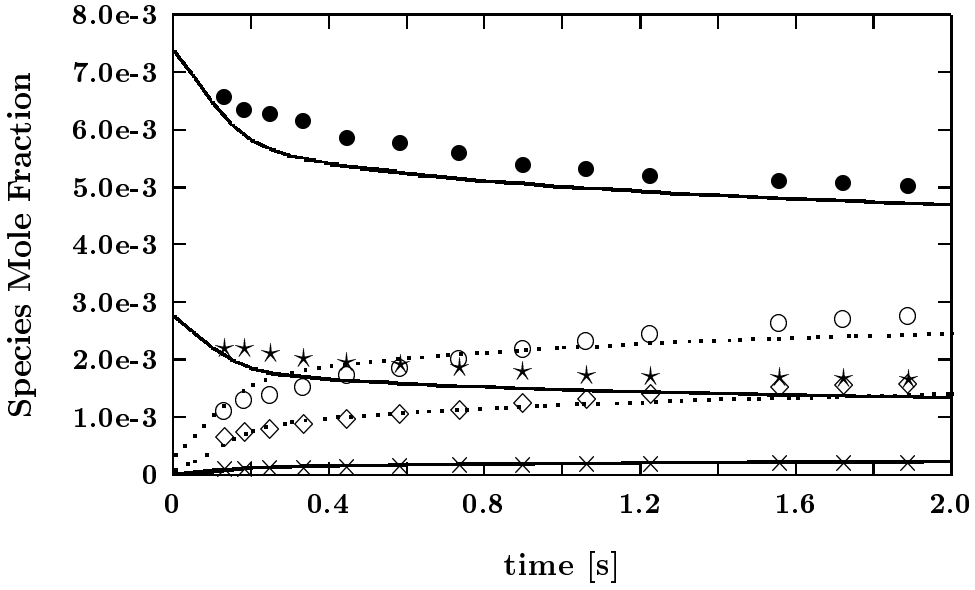

Figure 5: Measured (symbols) and calculated (curves) species concentrations from a flow reactor. 3080 ppm DME, $\phi = 1.18$, P=12.5 atm, T=593 K. • O_2, ∘ H_2O, ⋆ CH_3OCH_3, ◇ CO, and × CO_2. $\tau_{\text{offset}} = -0.3$ s. Dotted lines correspond to open symbols.

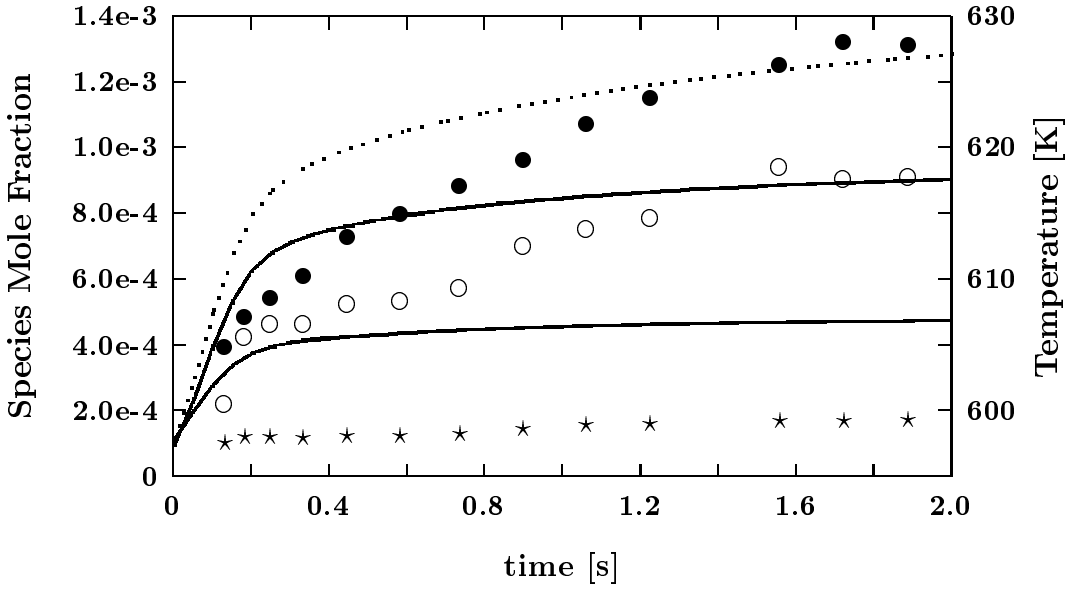

Figure 6: Measured (symbols) and calculated (curves) species concentrations from a flow reactor. 3080 ppm DME, $\phi = 1.18$, P=12.5 atm, T=593 K. • HOCHO, ∘ Temperature, and ⋆ CH_2O. $\tau_{\text{offset}} = -0.3$ s. Dotted lines correspond to open symbols.

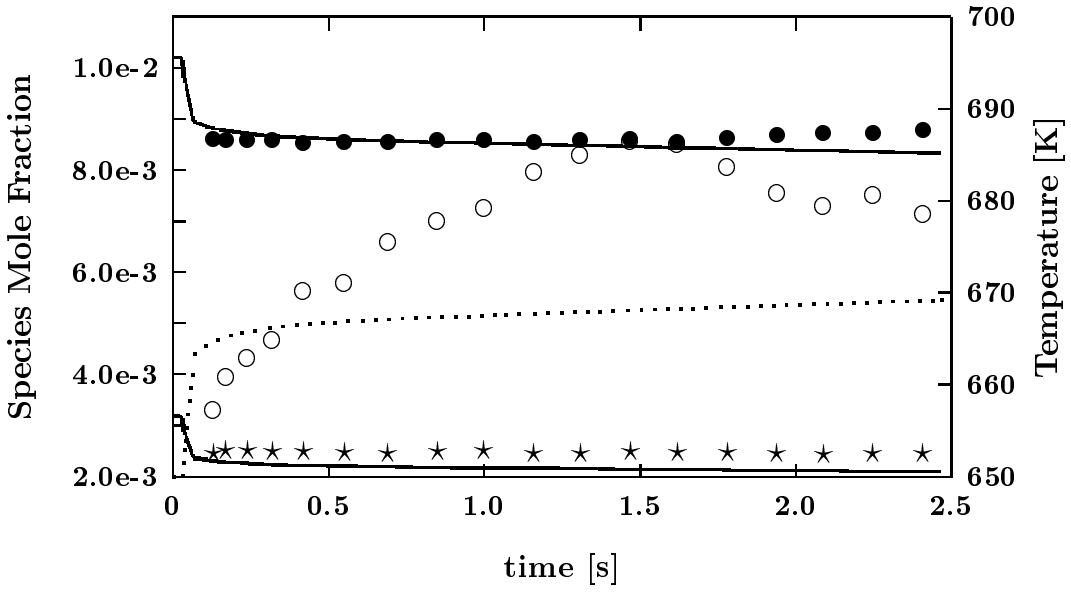

Figure 7: Measured (symbols) and calculated (curves) species concentrations from a flow reactor. 3190 ppm DME, $\phi = 0.93$, P=12.5 atm, T=650 K. $\bullet$ O_2, $\circ$ Temperature, and $\star$ CH_3OCH_3. Dotted lines correspond to open symbols.

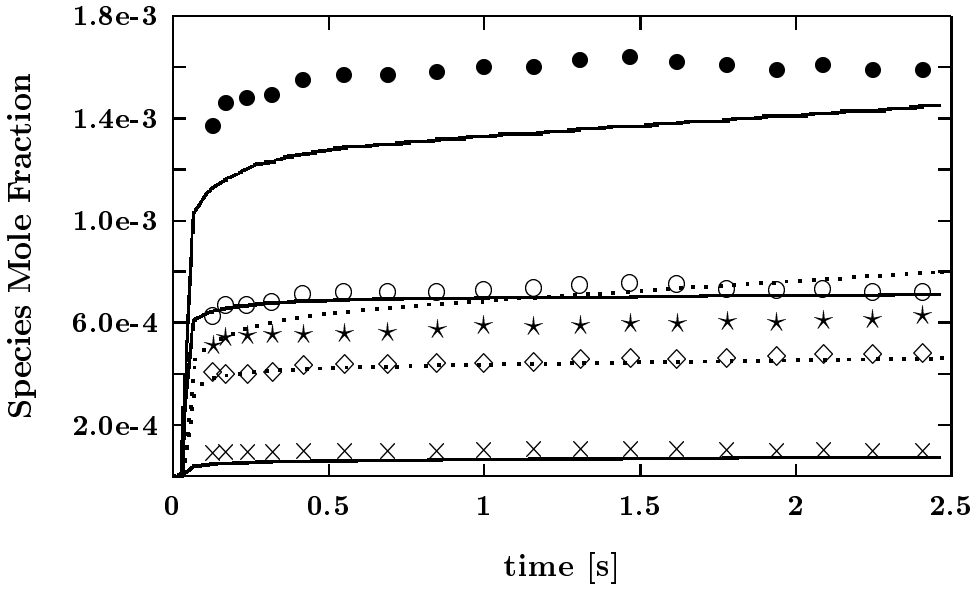

Figure 8: Measured (symbols) and calculated (curves) species concentrations from a flow reactor. 3190 ppm DME, $\phi = 0.93$, P=12.5 atm, T=650 K. $\bullet$ H_2O, $\circ$ CO, $\star$ CH_2O, $\diamond$ HOCHO and $\times$ CO_2. Dotted lines correspond to open symbols.

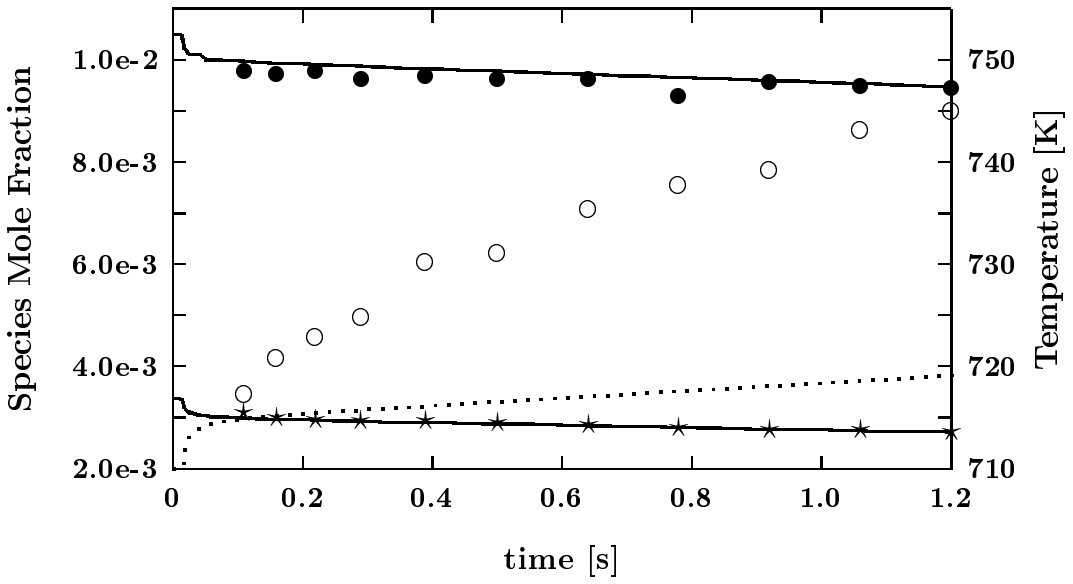

Figure 9: Measured (symbols) and calculated (curves) species concentrations from a flow reactor. 3380 ppm DME, ϕ = 0.97, P=12.5 atm, T=710 K. • O_2, ∘ Temperature, and ⋆ CH_3OCH_3. Dotted lines correspond to open symbols.

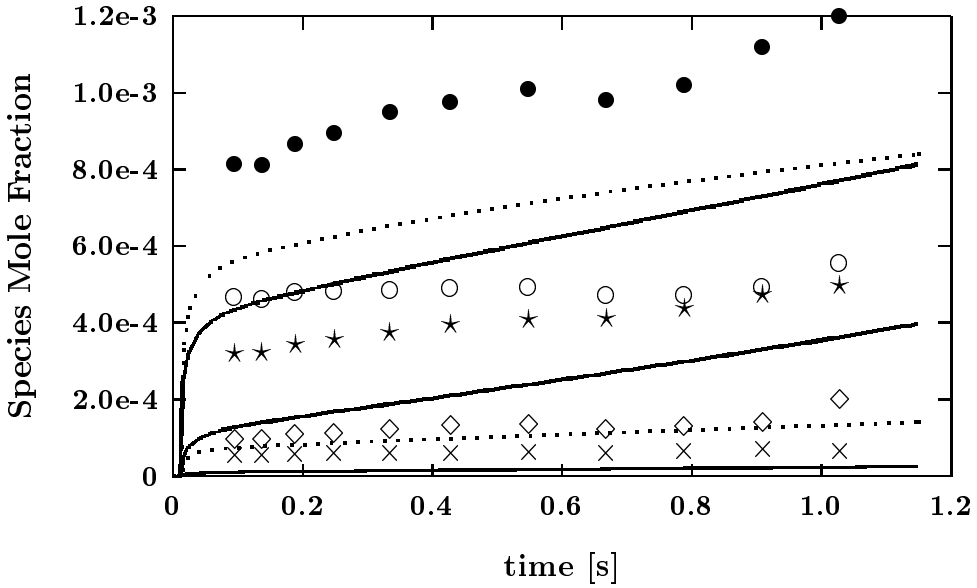

Figure 10: Measured (symbols) and calculated (curves) species concentrations from a flow reactor. 3380 ppm DME, $\phi = 0.97$, P=12.5 atm, T=710 K. • H_2O, ∘ CH_2O, ⋆ CO, ◇ HOCHO and × CO_2. Dotted lines correspond to open symbols.

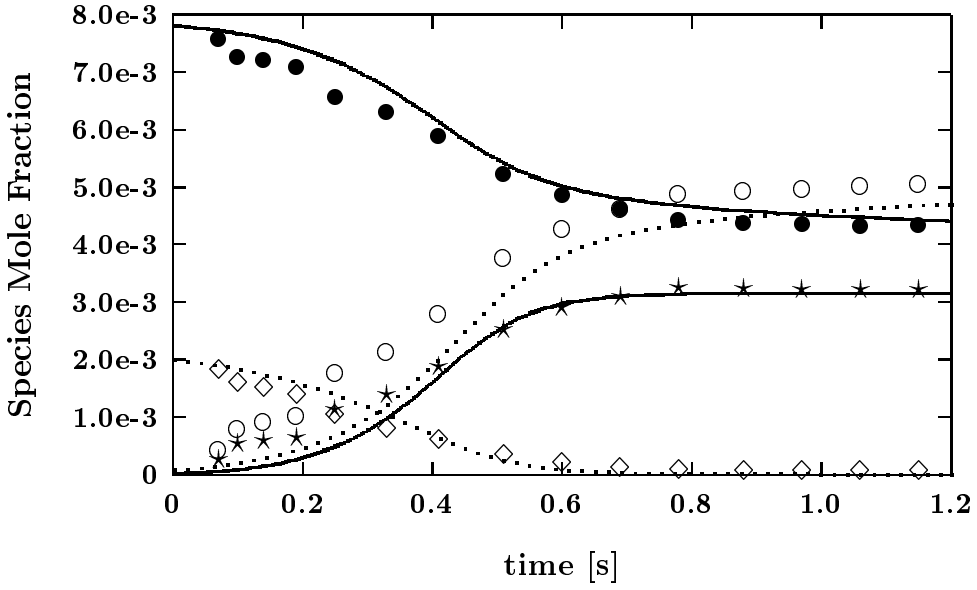

Figure 11: Measured (symbols) and calculated (curves) species concentrations from a flow reactor. 2130 ppm DME, $\phi = 0.81$, P=12 atm, T=849 K. • O_2, ∘ H_2O, ⋆ CO, and ◇ CH_3OCH_3. $\tau_{\text{offset}} = -0.2$ s. Dotted lines correspond to open symbols.

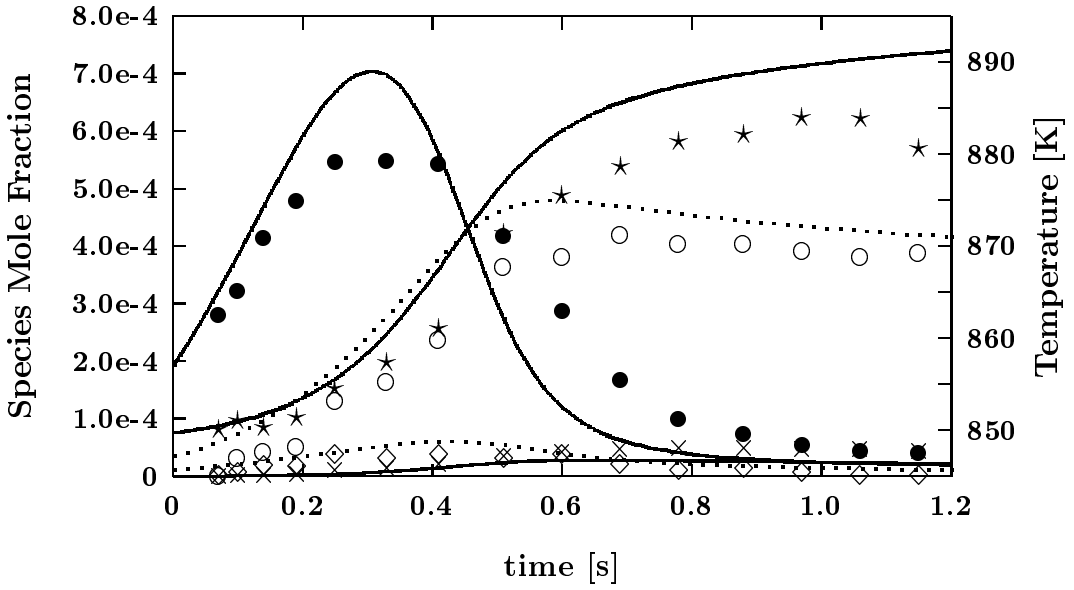

Figure 12: Measured (symbols) and calculated (curves) species concentrations from a flow reactor. 2130 ppm DME, $\phi = 0.81$, P=12 atm, T=849 K. • CH_2O, ∘ CH_4, ⋆ Temperature, ◇ C_2H_6 and × C_2H_4. $\tau_{\text{offset}} = -0.2$ s. Dotted lines correspond to open symbols.

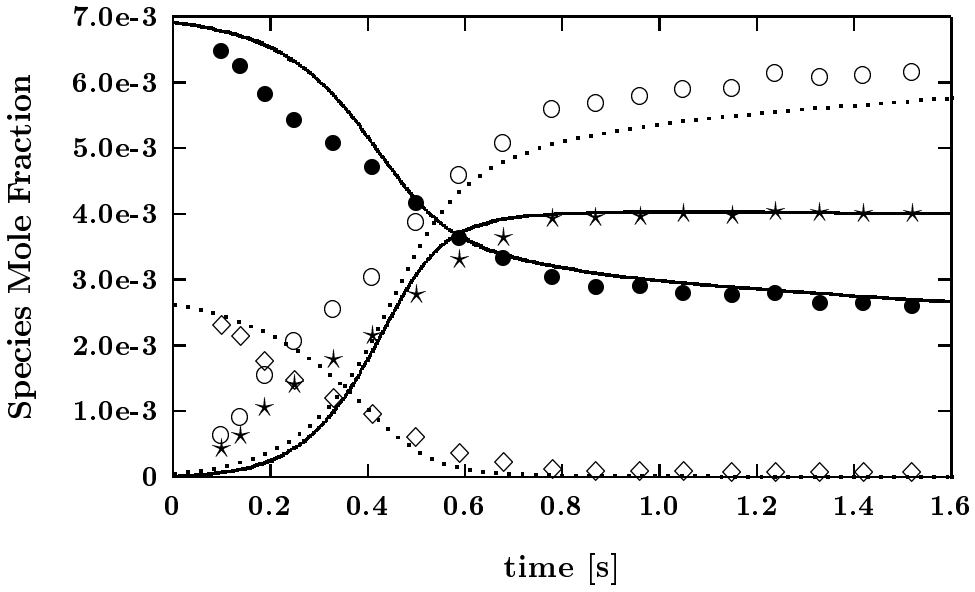

Figure 13: Measured (symbols) and calculated (curves) species concentrations from a flow reactor. 2730 ppm DME, $\phi = 1.17$, P=12 atm, T=849 K. • O_2, ∘ H_2O, ⋆ CO, and ◇ CH_3OCH_3. $\tau_{\text{offset}} = -0.15$ s. Dotted lines correspond to open symbols.

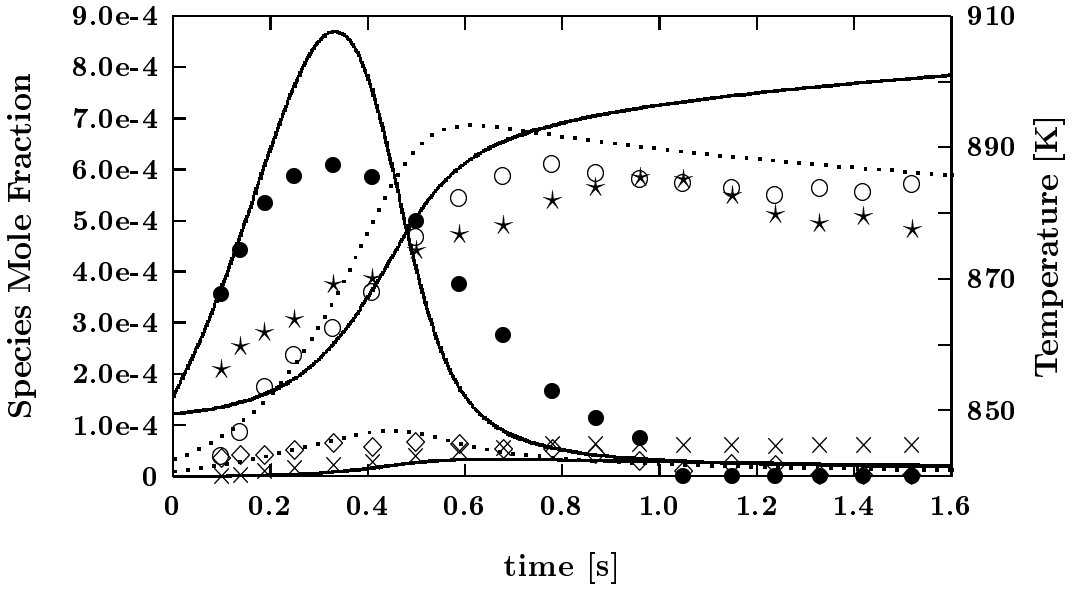

Figure 14: Measured (symbols) and calculated (curves) species concentrations from a flow reactor. 2730 ppm DME, $\phi = 1.17$, P=12 atm, T=849 K. • CH_2O, ∘ CH_4, ⋆ Temperature, ◇ C_2H_6, and × C_2H_4. $\tau_{\text{offset}} = -0.15$ s. Dotted lines correspond to open symbols.

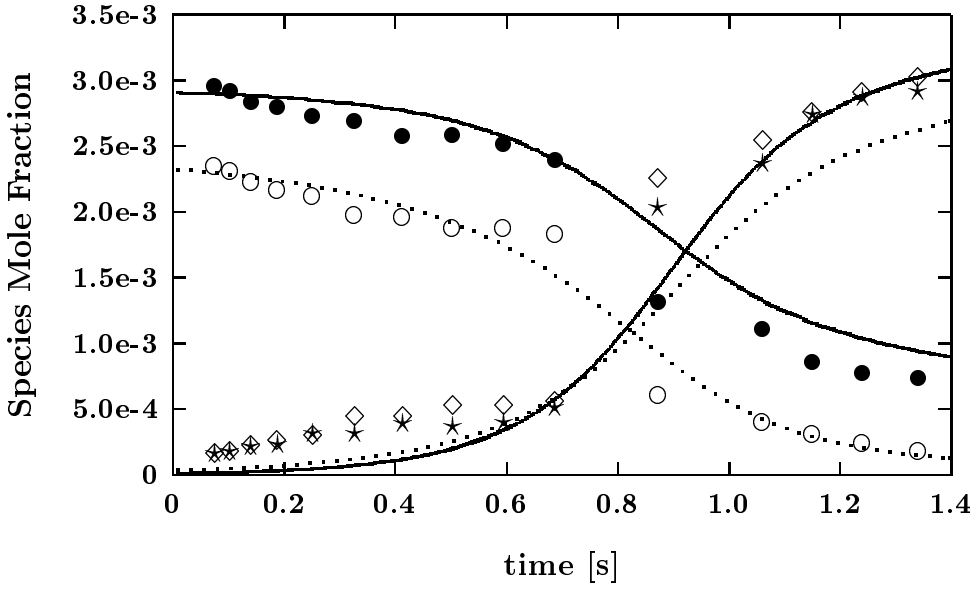

Figure 15: Measured (symbols) and calculated (curves) species concentrations from a flow reactor. 2430 ppm DME, $\phi = 2.48$, P=12 atm, T=852 K. • O_2, ∘ CH_3OCH_3, ⋆ CO, and ◇ H_2O. $\tau_{\text{offset}} = -0.5$ s. Dotted lines correspond to open symbols.

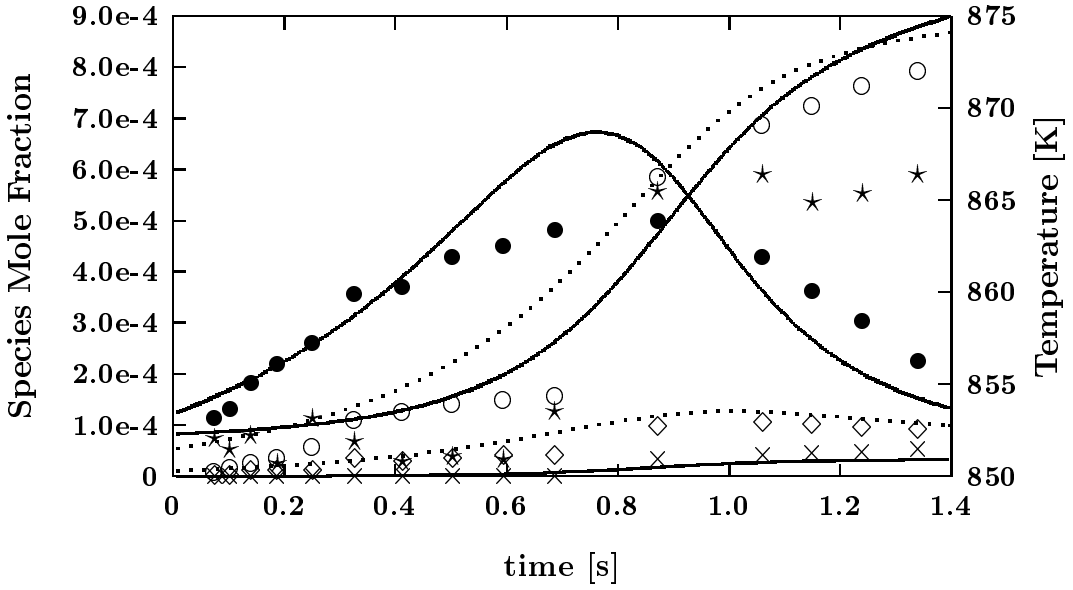

Figure 16: Measured (symbols) and calculated (curves) species concentrations from a flow reactor. 2430 ppm DME, $\phi = 2.48$, P=12 atm, T=852 K. • CH_2O, ∘ CH_4, ⋆ Temperature, ◇ C_2H_6, and × C_2H_4. $\tau_{\text{offset}} = -0.5$ s. Dotted lines correspond to open symbols.

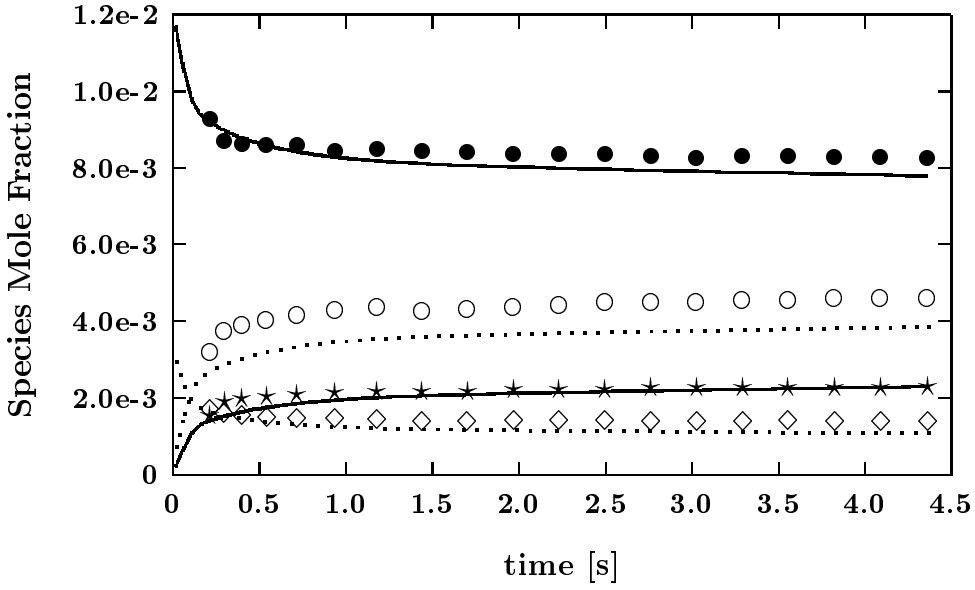

Figure 17: Measured (symbols) and calculated (curves) species concentrations from a flow reactor. 3580 ppm DME, $\phi = 0.85$, P=17 atm, T=600 K. • O_2, ∘ H_2O, ⋆ CO, and ◇ CH_3OCH_3. $\tau_{\text{offset}} = -0.2$ s. Dotted lines correspond to open symbols.

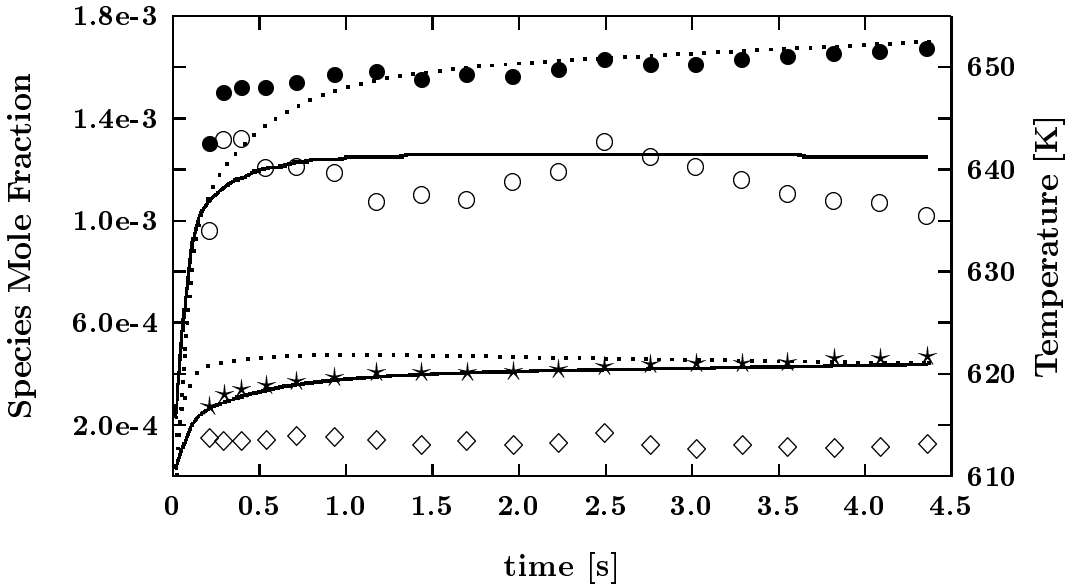

Figure 18: Measured (symbols) and calculated (curves) species concentrations from a flow reactor. 3580 ppm DME, $\phi = 0.85$, P=17 atm, T=600 K. • HOCHO, ∘ Temperature, ⋆ CO_2, and ◇ CH_2O. $\tau_{\text{offset}} = -0.2$ s. Dotted lines correspond to open symbols.

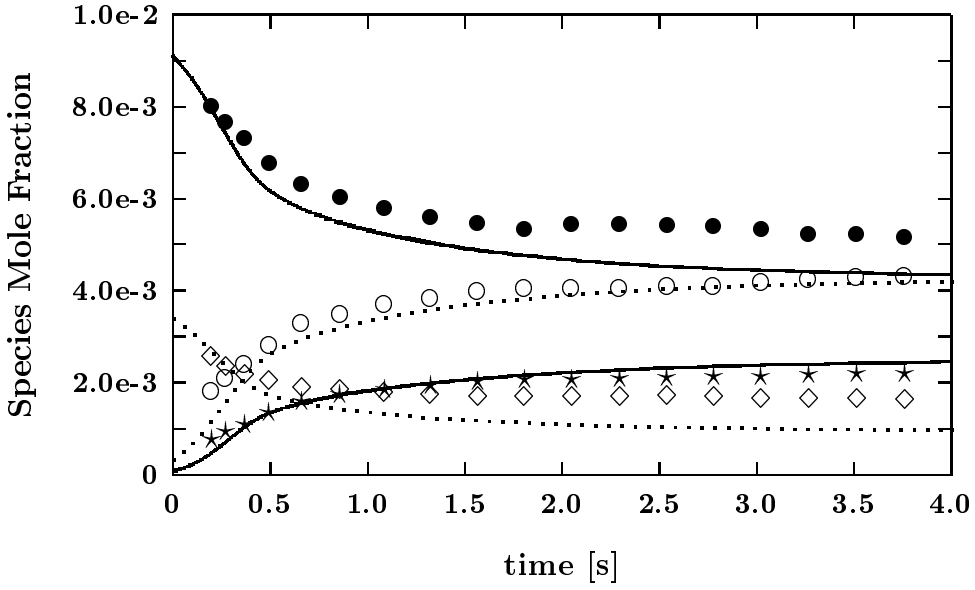

Figure 19: Measured (symbols) and calculated (curves) species concentrations from a flow reactor. 3700 ppm DME, $\phi = 1.16$, P=18 atm, T=580 K. • O_2, ○ H_2O, ⋆ CO, and ◇ CH_3OCH_3. $\tau_{\text{offset}} = -0.5$ s. Dotted lines correspond to open symbols.

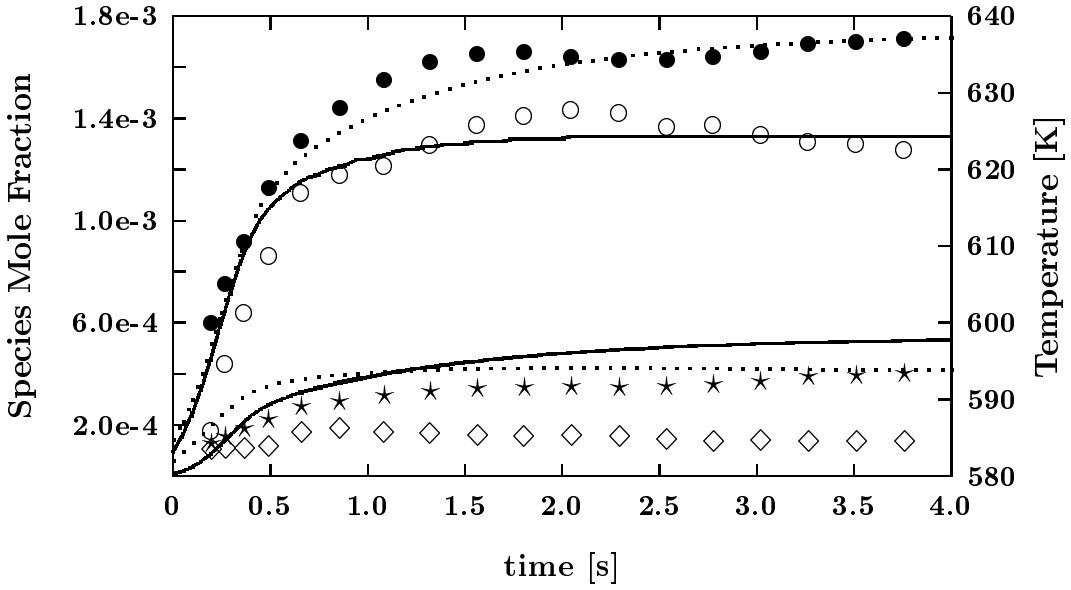

Figure 20: Measured (symbols) and calculated (curves) species concentrations from a flow reactor. 3700 ppm DME, $\phi = 1.16$, P=18 atm, T=580 K. • HOCHO, ○ Temperature, ⋆ CO_2, and ◇ CH_2O. $\tau_{\text{offset}} = -0.5$ s. Dotted lines correspond to open symbols.

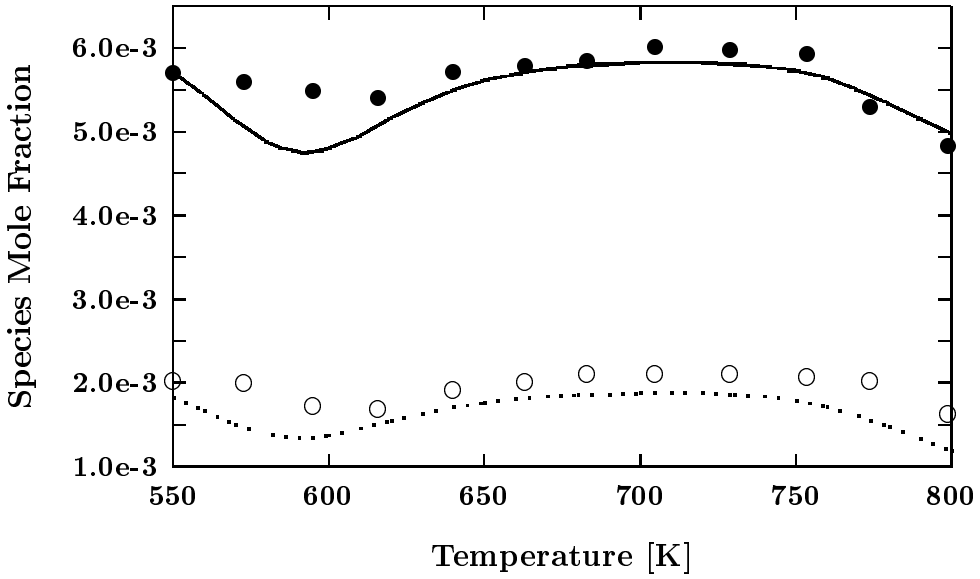

Figure 21: Experimental JSR results (points) [2] versus model predictions (lines) at 0.2% DME, $\phi = 1.0$, P=10 atm, τ=1 s. • O_2 and ∘ CH_3OCH_3. Dotted lines correspond to open symbols.

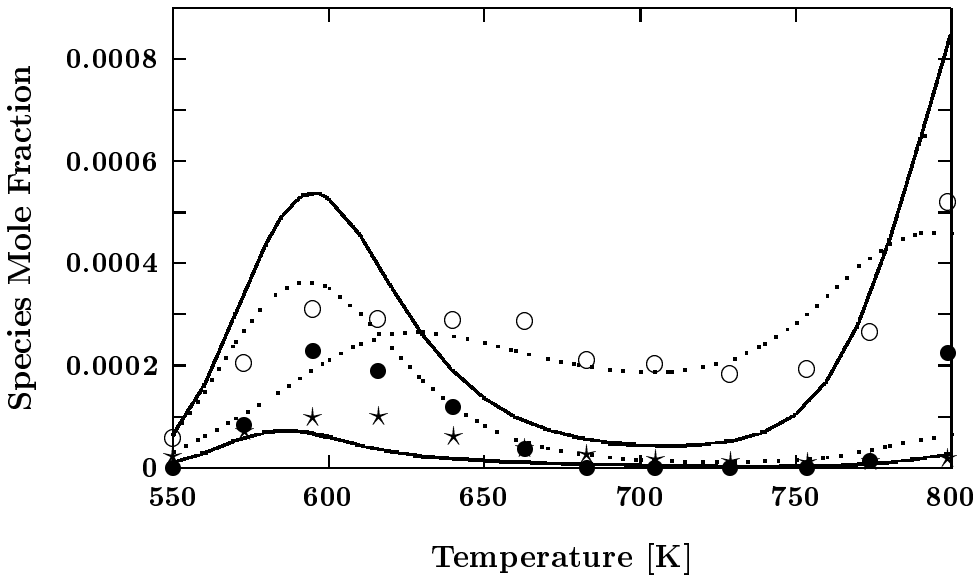

Figure 22: Experimental JSR results (points) [2] versus model predictions (lines) at 0.2% DME, $\phi = 1.0$, P=10 atm, τ=1 s. • CO, ∘ CH_2O, ⋆ CO_2, and ⋯ HOCHO (prediction only). Dotted lines correspond to open symbols.

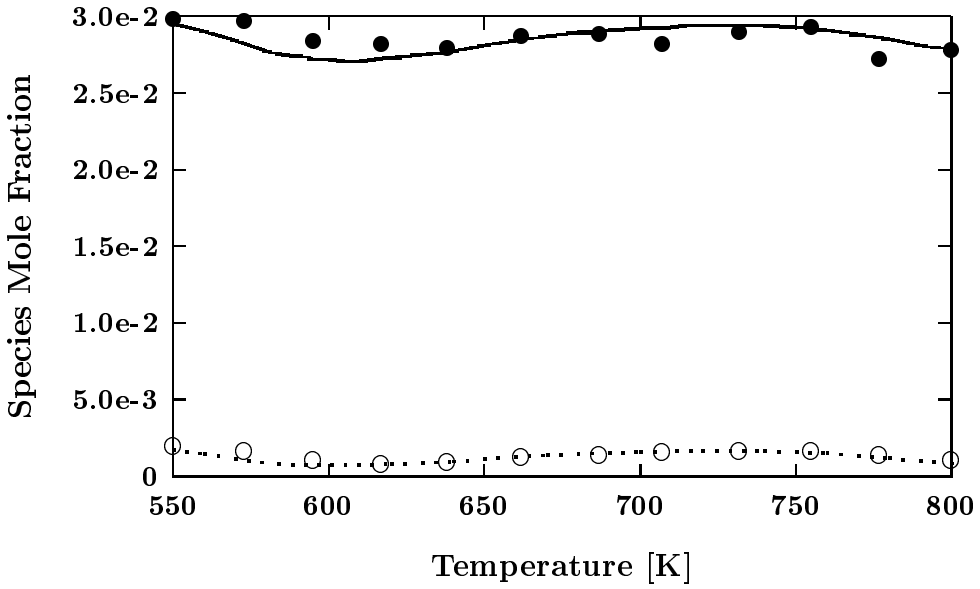

Figure 23: Experimental JSR results (points) [2] versus model predictions (lines) at 0.2% DME, $\phi = 0.2$, P=10 atm, τ=1 s. • O_2 and ∘ CH_3OCH_3. Dotted lines correspond to open symbols.

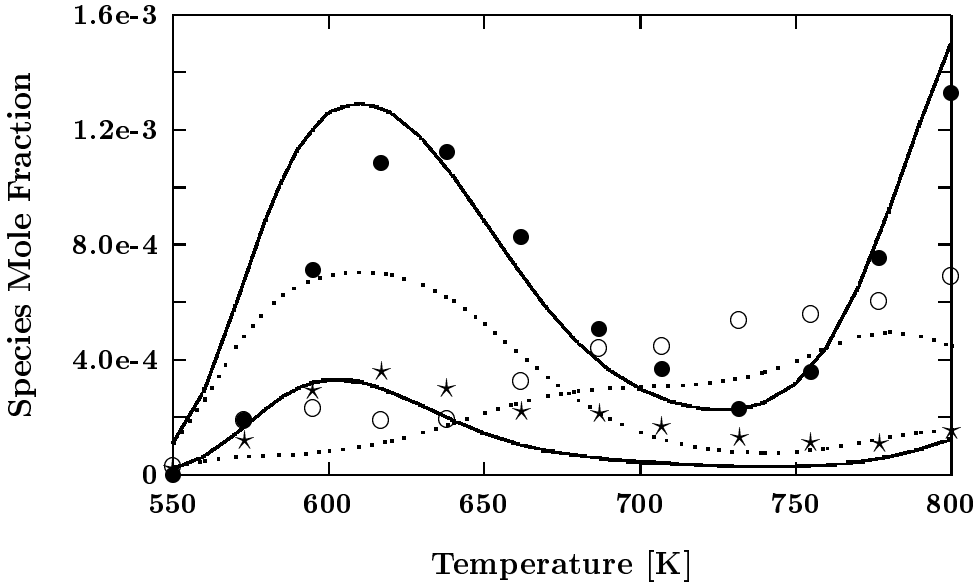

Figure 24: Experimental JSR results (points) [2] versus model predictions (lines) at 0.2% DME, $\phi = 0.2$, P=10 atm, τ=1 s. • CO, ∘ CH_2O, ⋆ CO_2, and ⋯ HOCHO (prediction only). Dotted lines correspond to open symbols.

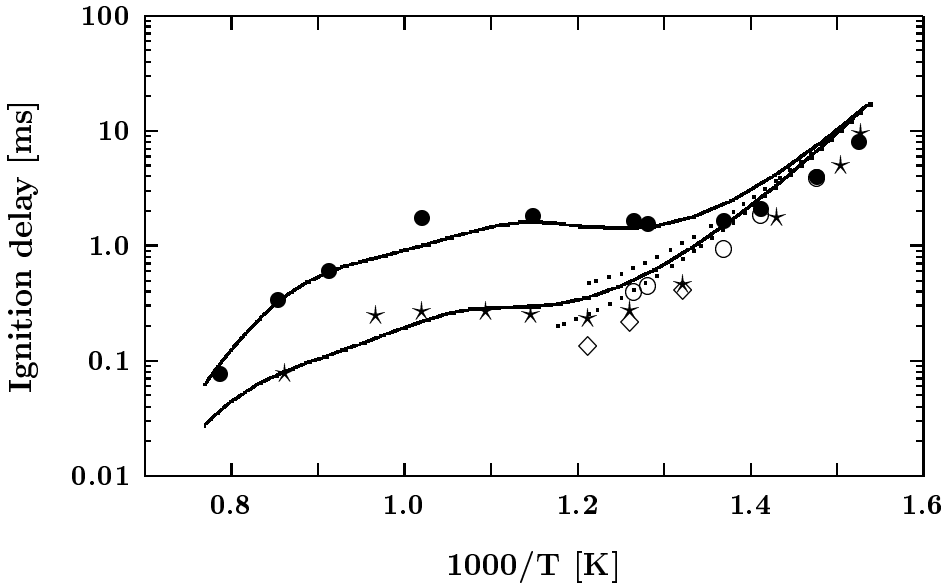

Figure 25: Experimental shock tube ignition delays (points) [3] versus model predictions (lines) for stoichiometric dimethyl ether oxidation in air. • total ignition, and ○ first stage ignition delay at 13 bar. ⋆ total ignition, and ◇ first stage ignition delay at 40 bar. Dotted lines correspond to open symbols.

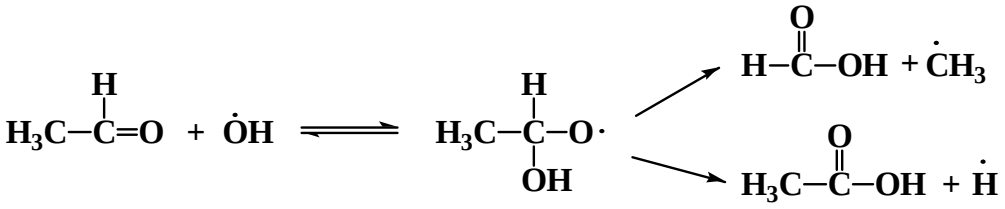

Figure 26: Possible routes of acetaldehyde oxidation by hydroxyl radicals.

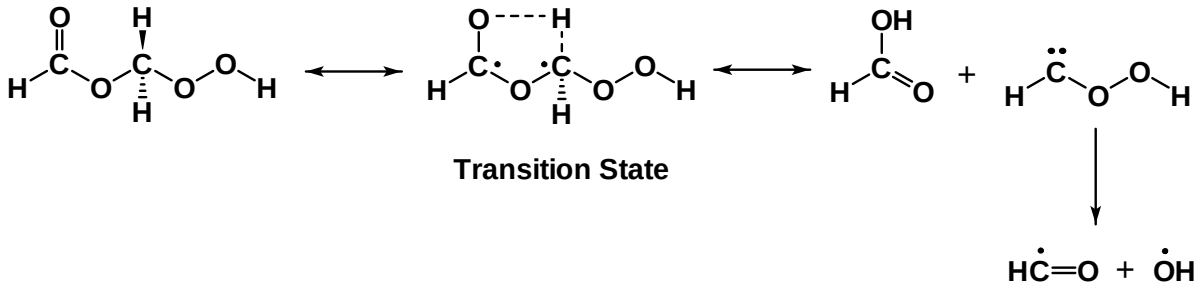

Figure 27: Alternative pathway for formic acid formation from HO_2CH_2OCHO.

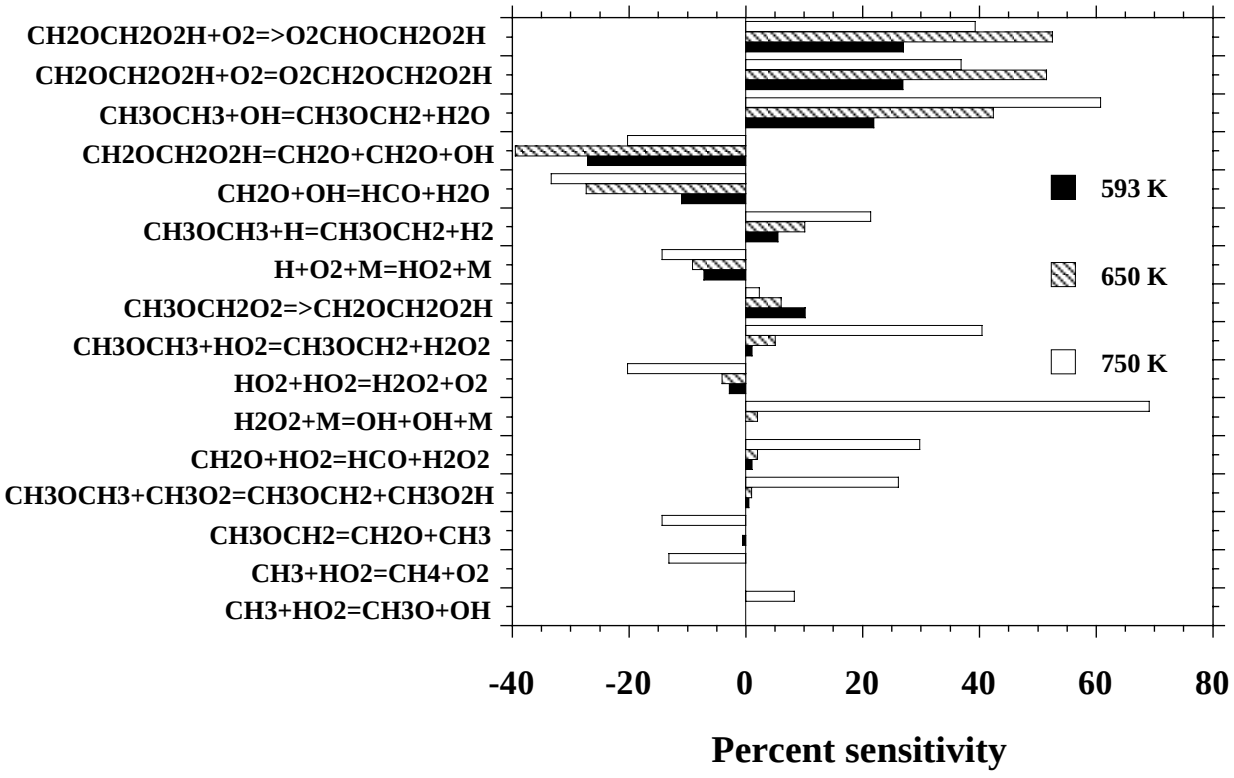

Figure 28: Sensitivity coefficients for dimethyl ether oxidation. 3030 ppm DME, $\phi = 1.19$, P=12.5 atm, τ=2.1 s.